



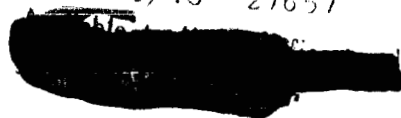
# APOLLO EXTENSION SYSTEMS

## METEOROID DESIGN DATA


(NASA-CR-153376) APOLLO APPLICATION  
SYSTEMS. VOLUME 2: A STUDY OF METEOROID  
DESIGN DATA FOR APOLLO APPLICATION SYSTEMS  
(Brown Engineering Co., Inc.) 93 2

N77-79929

00/13 Unclass  
27657



<del>X-66-37596</del>	X-67-70555
93	
CR-77423	2A
	32

**BROWN**  **ENGINEERING CO. INC.**  
**SYSTEM ENGINEERING DEPARTMENT**  
**HUNTSVILLE, ALABAMA**

RQ738565

APOLLO APPLICATION SYSTEMS

A STUDY OF  
METEOROID DESIGN DATA FOR APOLLO APPLICATION  
SYSTEMS  
by

Brownie Johnson

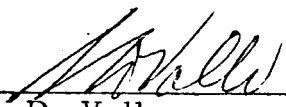
Prepared under  
Contract No. NAS 8-20073

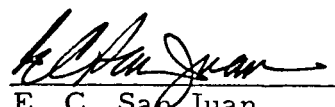
for

Spacecraft and Payload Systems Group  
Advanced Studies Office  
Propulsion and Vehicle Engineering Laboratory  
National Aeronautics and Space Administration  
George C. Marshall Space Flight Center  
Huntsville, Alabama

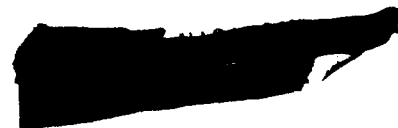
APPROVED

APPROVED

  
\_\_\_\_\_  
S. D. Vollo  
Program Manager  
Advanced Studies Department

  
\_\_\_\_\_  
E. C. San Juan  
Project Manager  
Base Development Branch

BROWN ENGINEERING COMPANY, INC.  
SPACE VEHICLE DIVISION  
HUNTSVILLE, ALABAMA



## PREFACE

This report was prepared by the System Integration Branch, Huntsville Operations Division of Brown Engineering Company, Inc. for the Marshall Space Flight Center. Efforts were performed under authorization of Technical Directive A2-ABX-003, Contract NAS 8-20073.

The NASA Technical Representatives were Mr. C. Darwin, Mr. J. H. Laue and A. Kromis of the Spacecraft and Payloads Group, Advanced Studies Office, Propulsion and Vehicle Engineering Laboratory (R-P&VE-AB).

The technical contributor was Mr. B. Johnson Jr.

## TABLE OF CONTENTS

<u>SECTION</u>	<u>TITLE</u>	<u>PAGE</u>
1.0	INTRODUCTION AND SUMMARY	1
2.0	OBJECTIVE	2
3.0	TASK OBJECTIVE	3
4.0	SURVEY AND COMPILATION OF DATA PERTAINING TO METEOROID SHIELDING DESIGNS	5
4.1	SPALLATION	12
4.2	MATERIAL CONSIDERATIONS	13
4.2.1	METEOROID SHIELDING BUMPER MATERIALS	13
4.2.1.1	CORRUGATED BUMPERS	18
4.2.2	ENERGY ABSORBANTS FOR APPLICATION TO MULTIPLE SHEET METEOROID SHIELDS	18
4.3	REVIEW OF EXPERIMENTAL METHODS AND DATA	22
4.3.1	HYPER-VELOCITY EXPERIMEN- TATION	22
4.3.2	STRESSED AND CRYOGENICALLY COOLED STRUCTURES	23
4.3.3	SIGNIFICANT STUDIES	24
4.3.3.1	THE IMPACT PROCESS	25
4.3.3.2	TARGET DYNAMIC DEFORMATION ANALYSIS	28
4.3.3.3	EFFECT OF PARTICLE SIZE	28

# TABLE OF CONTENTS (cont'd)

<u>SECTION</u>	<u>TITLE</u>	<u>PAGE</u>
4.3.3.4	SHEET SPACING	29
4.3.3.5	EFFECT OF PRE-TENSIONING THE BACKUP SHEET	29
4.3.3.6	MOMENTUM MULTIPLICATION	31
4.3.3.7	MULTIPLE BACKUP SHEETS IN METEOROID SHIELDING STRUCTURES	31
4.3.3.8	METEOROID SHIELD DETERMINATION	33
4.4	MICROMETEOROID PARTICLE CHARACTERISTICS	33
4.5	THEORETICAL METEOROID FLUX AND PENETRATION MODEL	38
4.5.1	NEAR-EARTH AND CISLUNAR METEOROID FLUX AND PUNCTURE MODEL	38
4.5.2	LUNAR SECONDARY PROJECTILE FLUX AND PUNCTURE MODEL	48
4.5.3	LUNAR AND NEAR-LUNAR PRIMARY METEOROID FLUX AND PUNCTURE MODEL	54
4.6	SINGLE-MULTIPLE SHEET METEOROID SHIELDING CORRELATION	61
4.7	CONCLUSIONS - MICROMETEOROID SHIELDING DESIGN	66
5.0	REFERENCES	

## LIST OF ILLUSTRATIONS

<u>FIGURE</u>	<u>TITLE</u>	<u>PAGE</u>
1-1	VARIATION OF TOTAL PENETRATION WITH IMPACT VELOCITY IN BUMPER PROTECTED TARGETS	6
1-2	EFFECTS OF BUMPER THICKNESS ON MAXIMUM METEOROID PENETRATION	7
1-3	BUMPER THICKNESS VS. MINIMUM TOTAL THICKNESS REQUIRED TO PREVENT COM- PLETE TARGET PENETRATION	8
1-4	MAXIMUM FRAGMENT VELOCITY VS. IMPACT VELOCITY	9
1-5	EFFECT OF BUMPER STANDOFF DIS- TANCE ON TOTAL METEOROID SHIELDING PENETRATION	10
1-6	BUMPER MATERIAL BARRIER EFFICIENCY	14
1-7	MATERIAL PROPERTIES	15, 16
1-8	EXAMPLE - COMPOSITE METEOROID SHIELDS	17
1-9	GLASS-WOOL PENETRATION CHARACTERISTICS	20, 21
1-9A	OPTIMUM SHIELD THICKNESS - ALUMINUM SHIELD AND PROJECTILE	26
1-9B	PRE-TENSIONED BEAM BEHAVIOR - CENTERLINE DISPLACEMENT VS. TIME	30
1-9C	PRE-TENSIONED BEAM BEHAVIOR - BACKUP THICKNESS VS. PRE-TENSIONED STRESS	32
1-9D	COMPARISON OF STRIP AND PLATE CALCULATIONS - APOLLO PARTICLE	34

# LIST OF ILLUSTRATIONS (cont'd)

<u>FIGURE</u>	<u>TITLE</u>	<u>PAGE</u>
1-9E	BACKUP THICKNESS NECESSARY TO PREVENT PENETRATION	35
1-10	PEGASUS EXPERIMENT - METEOROID PUNCTURE ANALYSIS	37
1-11	FLUX $F_s$ WITH MASS EQUAL TO OR GREATER THAN $m$ GRAMS AT $h$ KILOMETERS ABOVE THE EARTH	42
1-12, 12A	NEAR EARTH AND CISLUNAR SPACE METEOROID SHIELD THICKNESS - 50% CONFIDENCE LEVEL	43, 44
1-13, 13A	NEAR EARTH AND CISLUNAR SPACE METEOROID SHIELD THICKNESS - 75% CONFIDENCE LEVEL	46, 47
1-14	LUNAR SECONDARY PARTICLE SHIELD THICKNESS	53
1-15, 15A	LUNAR PRIMARY METEOROID SHIELD THICKNESS - 50% CONFIDENCE LEVEL	59, 60
1-16, 16A	LUNAR PRIMARY METEOROID SHIELD THICKNESS - 75% CONFIDENCE LEVEL	62, 63
1-17	VARIATION OF TARGET BALLISTIC LIMIT AS A FUNCTION OF THE NUMBER OF PROTECTIVE SHEETS	65
1-18	METEOROID SHIELDING EFFICIENCY FACTORS	67, 68

## ABBREVIATIONS

AAP	- Apollo Application Program
LEM	- Lunar Excursion Module
LEM/T	- Lunar Excursion Module/Truck
MOLAB	- Lunar Mobile Laboratory
LSV	- Lunar Surface Vehicle
LSSM	- Lunar Scientific Survey Module
LFV	- Lunar Flying Vehicle
MSFC	- Marshall Space Flight Center
MILA	- Merritt Island Launch Area
KSC	- Kennedy Space Center



## DEFINITIONS

- SLM                      Shelter Laboratory Module (SLM) or Lunar Shelter Laboratory (SHELAB) represented here is considered to be a lightweight structure attached to the LEM/T structure, capable of providing a scientific laboratory environment, and shelter for two or more astronauts under lunar environmental hazards.
- LSV                      Lunar Surface Vehicle (LSV) is considered to be a wheeled, transportable, lightweight, self-propelled vehicle which provides transportation for the astronauts and carry scientific instrumentation required for lunar exploration and survey.
- LFV                      The Lunar Flying Vehicle (LFV) is considered to be a two-man, transportable, lightweight, self-propulsion vehicle which will provide flying transportation for the astronauts' use for exploring in accessible areas and in case of an emergency.

## DEFINITIONS (Cont'd)

## LEM TRUCK

The Lunar Excursion Module/Truck (LEM/T) is the automated unmanned version of the LEM descent stage designed to transport lunar payloads from orbit to the lunar surface.

## LAUNCH VEHICLE

The Launch Vehicle is the Saturn V, composed of the S-IC booster stage, the S-II stage, the S-IVB stage, and IU Instrument Unit (IU).

## MOLAB

Lunar Mobile Laboratory - A combined shelter-mobile laboratory vehicle equipped scientific instruments and necessary equipment for lunar survival.

## ALSS

The Apollo Logistics Support System (ALSS) consists of the Launch Vehicle, the spacecraft, the flight crew, the ground support systems, and the assigned payload.

## DEFINITIONS (Cont'd)

## GROUND RULES

Ground rules are defined as criteria or conditions which must be used as limits for concept design and as the basis for concept evaluation.

## ASSUMPTIONS

Assumptions are defined as assumed criteria or conditions which are used as study guidelines. Assumptions must be within the limits of the ground rules.

## SECTION 1.0

## INTRODUCTION AND SUMMARY

The lunar scientific exploration phases proposed under the Apollo Application Program and subsequent programs will utilize many structural systems which will include orbital modules, fixed shelters, large mobile laboratories, flying devices, small roving vehicles, and emergency survival shelters. In each case the environmental constraints to be encountered during the programmed missions will be considered when structural designs are established.

In the specific area of meteoroid shielding numerous studies, both theoretical and experimental, have been performed. A deficiency, thus far, has been the practical application of previous studies in such a manner that a prospective designer can easily determine optimum meteoroid shielding designs for the near-earth, Cislunar, and Lunar environment.

## SECTION 2.0

## OBJECTIVE

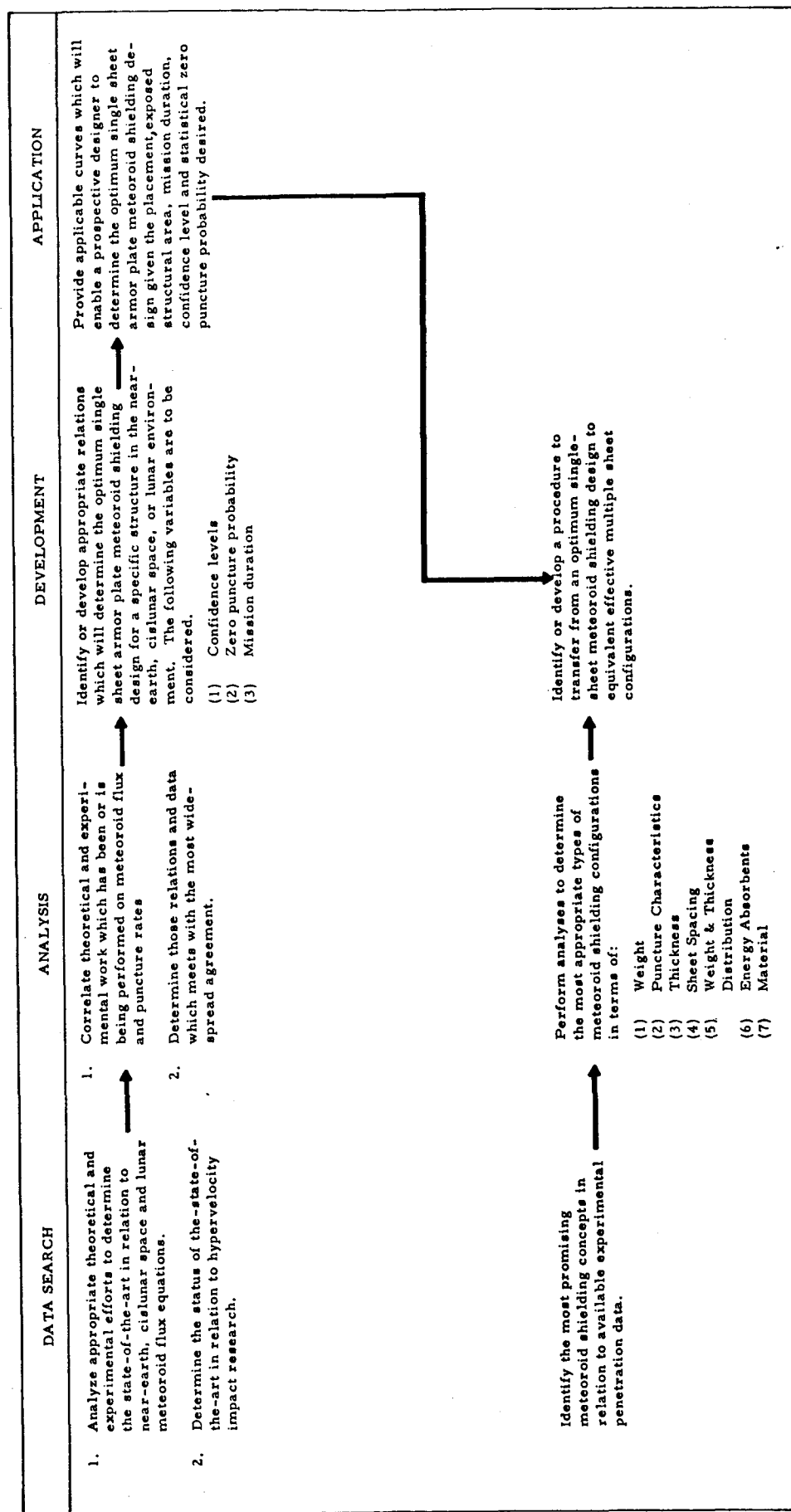
The purpose of this report will be to accomplish the following in support of the Apollo Application Program.

- (1) Analyze the most recent technical reports available to arrive at near-earth, cislunar space, and lunar meteoroid flux and penetration relations which meet with the most wide spread agreement.
- (2) Correlate theoretical and experimental work on meteoroid flux and penetration rates.
- (3) Provide applicable curves through which a designer may determine the optimum single sheet meteoroid shield for near-earth, cislunar space and lunar environments.
- (4) Provide applicable curves or procedures to determine the effective equivalent multiple sheet meteoroid shielding design when given the best single sheet configuration.
- (5) Analyze appropriate technical reports and references to determine which type of wall design will be most appropriate taking under consideration (a) total weight, (b) meteoroid flux and penetration rates, (c) sheet thicknesses, (d) optimum sheet spacing, distribution of weight between front and back sheets in multiple-sheet structure and sheet material (Physical Characteristics).

## SECTION 3.0

### TASK APPROACH

The approach taken in the establishment of a meteoroid shielding design criteria was to prepare an overall task methodology as illustrated on page 4 .



TASK METHODOLOGY CHART

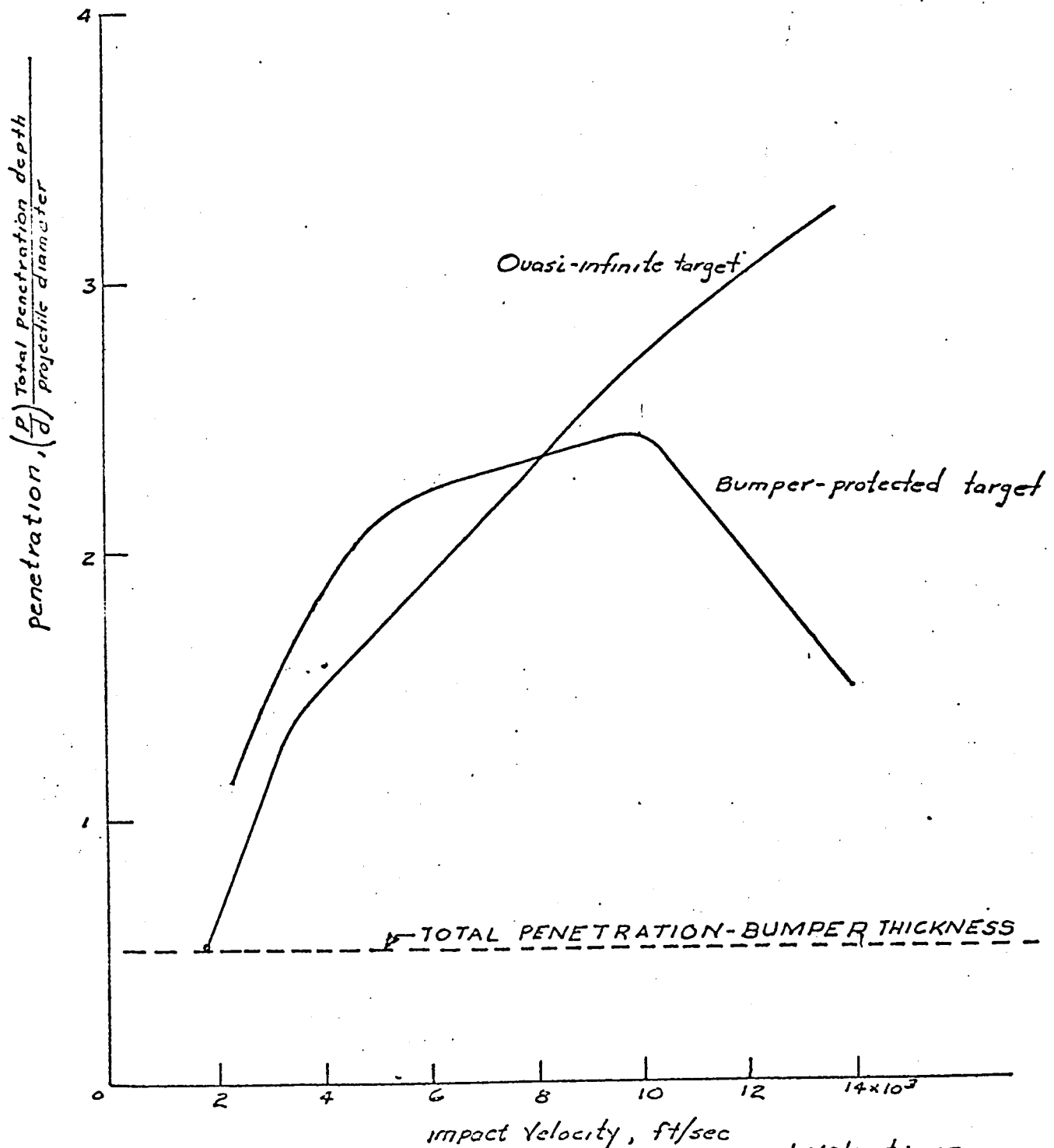
## SECTION 4.0

## SURVEY AND COMPILATION OF DATA PERTAINING TO METEOROID SHIELDING DESIGNS

In reviewing references which deal with the general subject of meteoroid protection for spacecraft and Lunar structures, it becomes apparent that there are conclusions which meet with general agreement. The conclusions which provide some basis for a meteoroid shielding design criteria are listed below. (See Figures 1-1, 1-2, 1-3, 1-4 and 1-5).

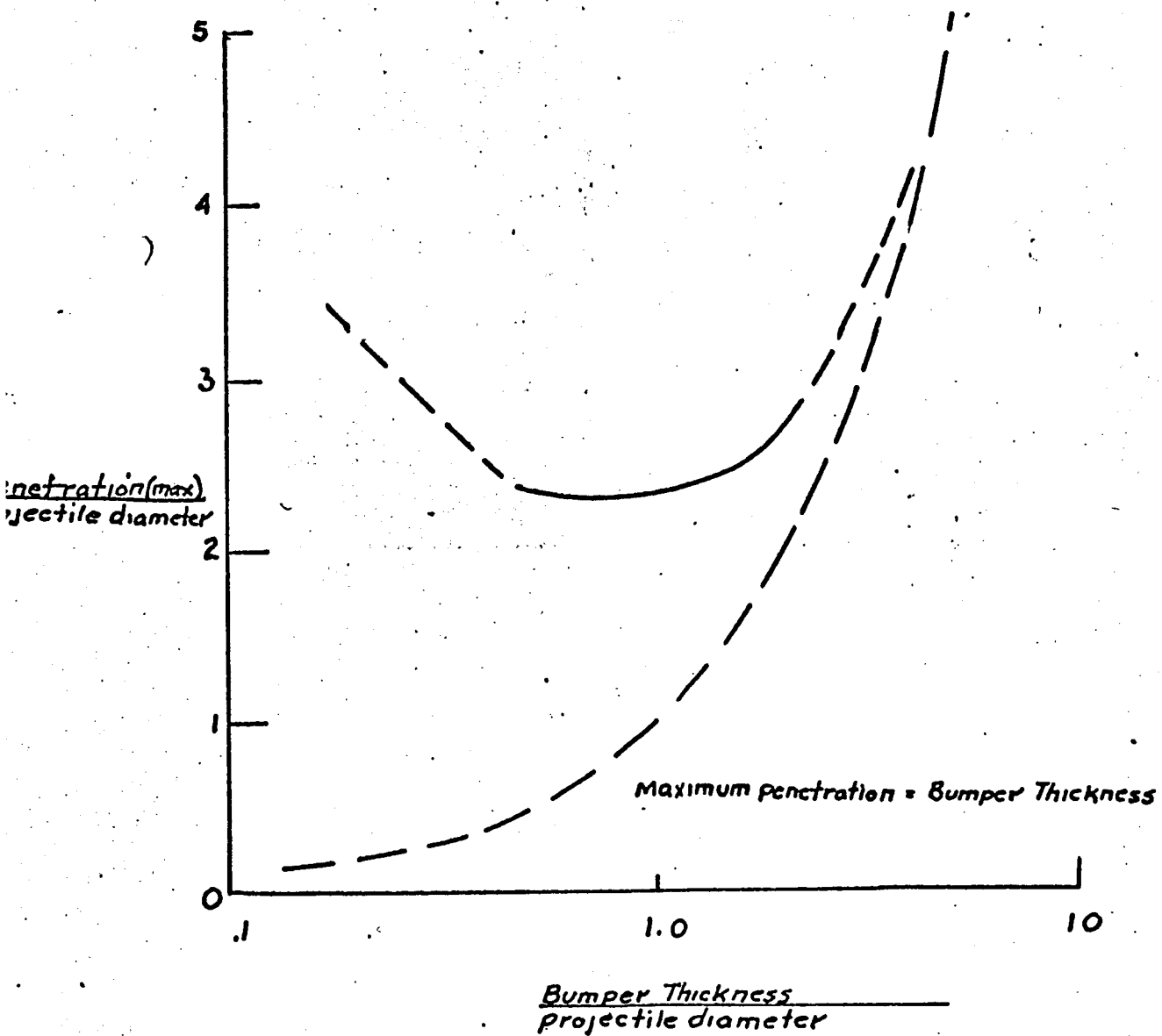
1. Per Reference (12) experimental evidence was obtained which indicates that the outer sheet of a multi-sheet structure serves primarily as a projectile break-up device fragmenting and dispersing the energy from the impacting particle. The energy extracted by the front sheet of a structure as the sheet thickness is increased does not correspond to the loss of energy absorbing capabilities of the rear sheet as the thickness is decreased. Consequently, the optimum meteoroid-resistant bumper will be just thick enough to completely fragment the projectile. Further, the conclusion was made that, for a given mass per unit area of meteoroid bumper, the bumper material is relatively unimportant.
2. Thicknesses of bumper materials per references (4) and (12) were found experimentally to be most appropriate when the thickness was 0.5 of the projectile diameter. (See Figures 1-2 and 1-3).
3. Impacting a bumper protected target was not effective when the projectile traveled in low velocity ranges. (See Figure 1-1) The velocity of which effectiveness was reached is dependent in part upon bumper thickness, particle velocity, and bumper standoff distance. Further, total penetration into a bumper protected target at low velocities is greater than in a quasi-infinite target (i. e., thick plate).
4. Total penetration into bumper protected target increased as impact velocity increased in low velocity range. (See Figure 1-1)
  - a. At 10,000 ft./sec. penetration reached a max. and decreased with further increase in impact velocity.
  - b. Bumper thickness was 0.5 projectile diameter.
  - c. Stand-off distance was 32 projectile diameters.





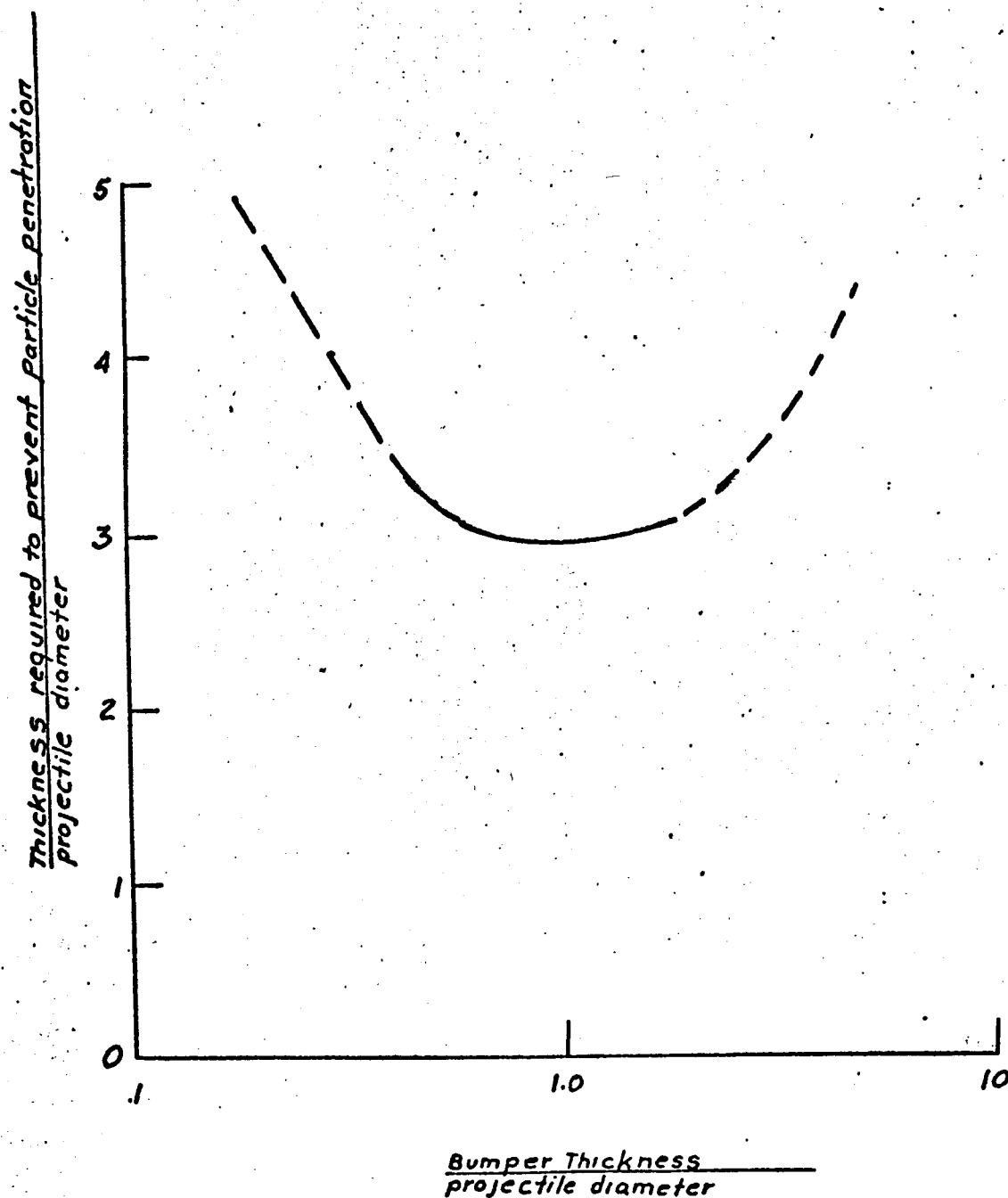
variation of total penetration with impact velocity in bumper protected target. Bumpers were 0.031 inch-thick 2024-T3 aluminum alloy at a standoff distance of 2 inches. Walls were 1-inch thick 2024-T4 aluminum alloy; Projectiles were 0.062-inch Diameter copper spheres.

FIGURE 1-1 VARIATION OF TOTAL PENETRATION WITH IMPACT VELOCITY IN BUMPER PROTECTED TARGETS



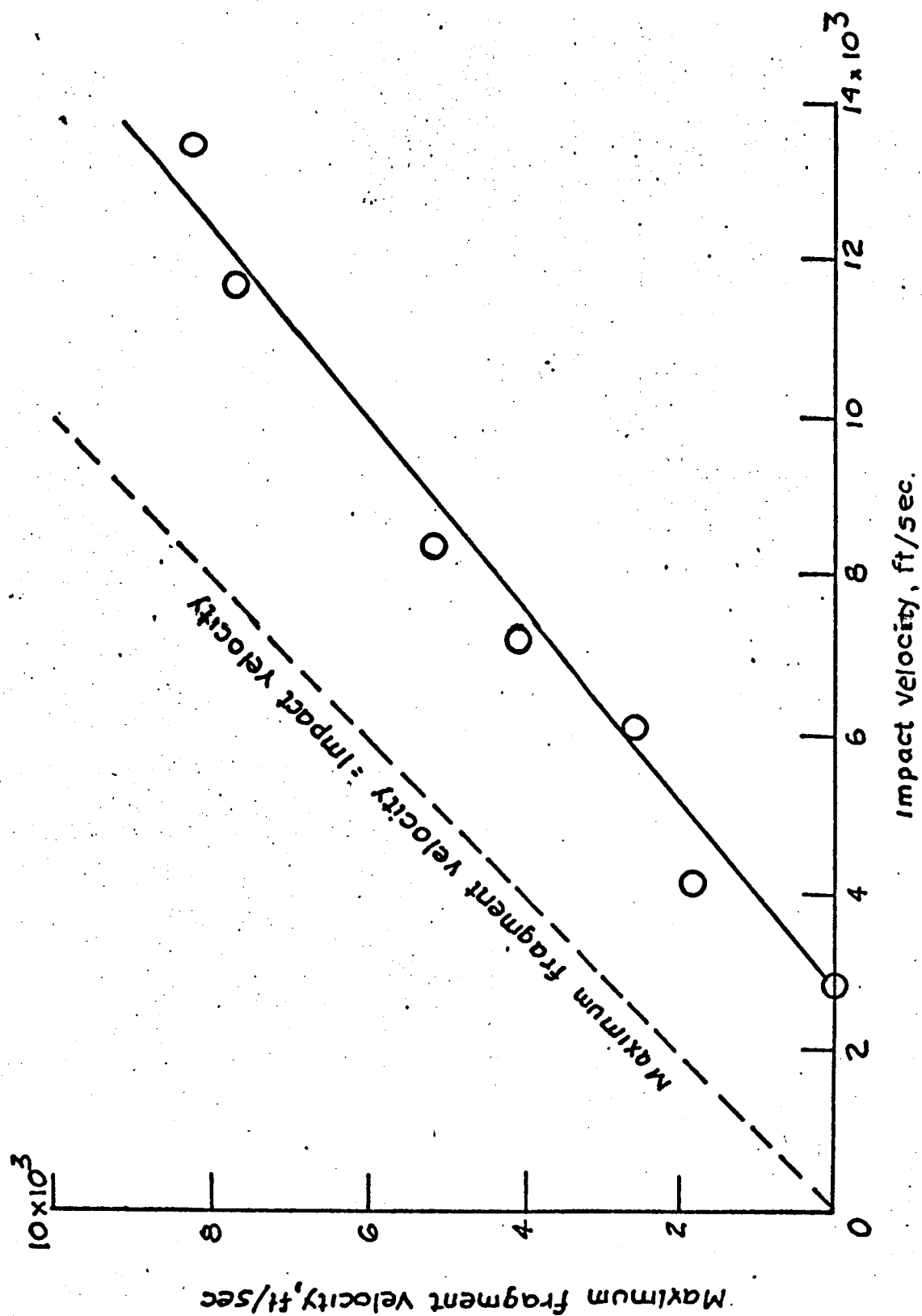
Effects of bumper thickness on maximum penetration. Bumpers - 2024-T3 aluminum alloy at a standoff distance greater than 8 projectile diameters; main walls - 1-inch-thick 2024-T4 aluminum alloy; projectiles - 0.062-inch-diameter copper spheres.

FIGURE 1-2 EFFECTS OF BUMPER THICKNESS ON MAXIMUM METEOROID PENETRATION



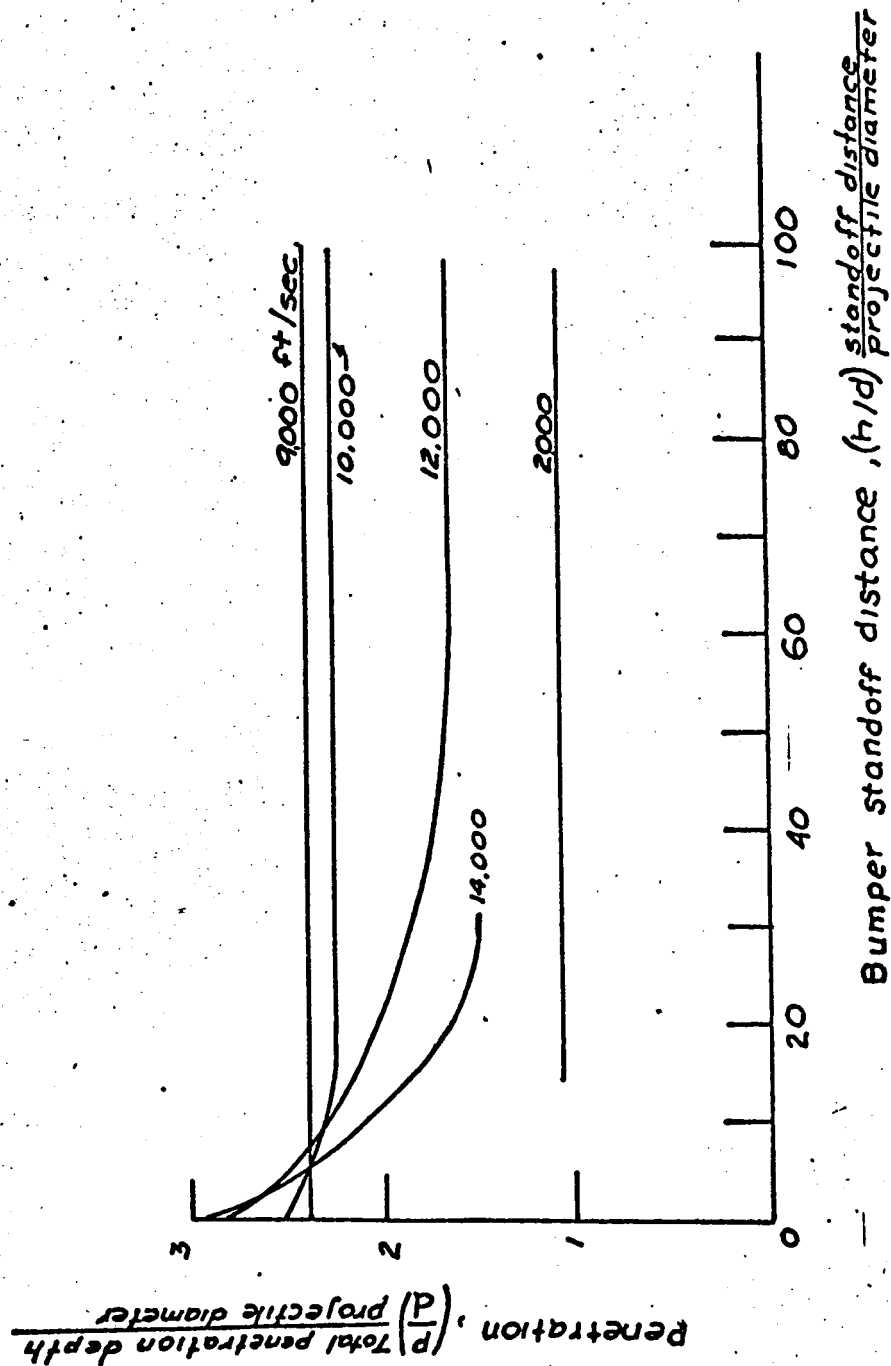
Calculated effect of bumper thickness on minimum total thickness required to prevent complete penetration of projectiles at any impact velocity in the velocity range from 0 to 15,000 ft/sec. Bumpers - 2024-T3 aluminum alloy at a stand off greater than 8 projectile diameters. Main walls - 1-inch thick 2024-T4 aluminum alloy; projectiles - 0.062-inch-diameter copper spheres.

FIGURE 1-3 BUMPER THICKNESS VS MINIMUM TOTAL THICKNESS REQUIRED TO PREVENT COMPLETE TARGET PENETRATION



Maximum fragment velocities observed at various impact velocities. Bumpers were 0.125 inch-thick 2024-T3 aluminum alloy; projectiles were 0.220 inch-diameter 2024-T4 aluminum-alloy spheres.

FIGURE 1-4 MAXIMUM FRAGMENT VELOCITY VS. IMPACT VELOCITY



Effect of bumper standoff distance on penetration. Bumpers were 0.031-inch-thick 2024-T3 aluminum alloy; main walls were 1-inch-thick 2024-T4 aluminum alloy; projectiles were 0.062-inch diameter copper spheres.

FIGURE 1-5 EFFECT OF BUMPER STANDOFF DISTANCE ON TOTAL METEOROID SHIELDING PENETRATION

5. Per reference 5, less momentum is required to penetrate a finite plate than is required to penetrate a quasi-infinite plate to a depth equal to a plate thickness. Consequently, a projectile which has penetrated a bumper has more momentum left than if it has penetrated a quasi-infinite target.
6. When the velocity of a meteoroid is not specified, the thickness of a just-puncturable wall is directly proportional to the cube root of the meteoroid mass and inversely proportional to the cube root of the product of the density and Brinell hardness of the wall material.
7. Max penetration - 9,950 ft/sec. projectiles shattered but remained clustered. (See Figure 1-1).
8. A stand-off distance of 50 times the projectile diameter took full advantage of fragment dispersion with velocities at 12,000 ft/sec. (See Figure 1-5).
9. A stand-off distance of 8 times the projectile diameter was required to cause total penetration to decrease with increasing impact velocities from 9,000 to 14,000 ft/sec. (See Figure 1-5).
10. At velocities too low to cause fragmentation of the projectile, the total penetration is independent of bumper stand-off distance.
11. Maximum penetration into bumper protected targets that had bumper thicknesses between 0.5 and 2.0 projectile diameters was less than that found in targets with either greater or less thicknesses. The bumper protected target that had a bumper thickness of 0.5 projectile diameter was the most effective in reducing penetration damage. (See Figures 1-2 and 1-3).
12. Data was obtained over a small range of meteor velocities. Indications are that in some instances the closing velocities may approach 200,000 ft/sec. The trends itemized below are subject to verification with high velocity gas guns but should hold true.
  - a. Penetration will continue to decrease as velocity increases until such time fragmentation and dispersion will be so complete that minor damage will occur to a main wall.

- b. Assuming (a) is true, the maximum penetration observed at 10,000 ft/sec. would be the absolute maximum penetration in velocity range of 0 to 200,000 ft/sec. (See Figure 1-1).
- 13. For stand-off distances less than 8 times the projectile diameter an increase in impact velocity always resulted in increased penetration.
- 14. At velocities great enough to cause fragmentation of the projectile the total penetration decreased with increased bumper stand-off distance.

#### 4.1 SPALLATION

Per reference 16, bumper design must be directed not only at efficiency in breaking up a projectile but also some consideration must be given to bumper spall. These larger fragments of bumper material although probably low in energy are potentially more dangerous than the more fragmented projectile. Bumper spall can be expected to be more extensive when the bumper is too thick. Since an average projectile size will have to be accounted for in bumper design criteria, it will be impossible to avoid a condition where a bumper will be too thick. On this basis it may be appropriate to revise the simple whipple bumper to include secondary spall shielding, particularly on the structure dome or roof. Possibly sufficient filler material will suffice and would result in considerable weight savings over another structural shell. In this respect, the density of both particle and projectile are the most important material properties affecting bumper performance. Figure 1-7 lists some applicable materials and their densities.

A significant number of the theoretical studies dealing with the effects of meteoroid impacts have proposed that at high velocities (in excess of 30,000 fps) only molten or vaporized material strikes the main pressure vessel wall. The most recent experimental efforts including reference (29) indicate that this is not the case. It has been determined that target material outside of the projectile diameter on impact is removed by a shearing action which begins at the projectile edge and moves outward. The shearing forces have their maximum at the edge of the impact zone and dissipate as the fragmented area grows. Consequently, no matter what the velocity of the impacting particle is, some of the bumper spall will be solid low velocity fragments. On this basis, the least damage would be caused by spall resulting from the lightest bumpers. Although not proven, several sources including

reference (29) have proposed that there is a relation between the degrees of spallation and the bumper material melting points. Indications are that meteoroid bumpers comprised of materials with lower melting points suffer less total penetration when impacted.

## 4.2 MATERIAL CONSIDERATIONS

The optimum selection of materials, both bumper and energy absorbers, has been one of the primary goals of experimental efforts performed in the area of meteoroid shielding research. The biggest obstacle, thus far, has been the testing of materials at true meteoroid velocities.

### 4.2.1 METEOROID SHIELDING BUMPER MATERIAL

Experimental results support the contention that for a given meteoroid shielding bumper material density the kind of material is of secondary importance. The density selected for application though is a factor to be considered for the reasons described in Section 1.2. Figure 1-6 represents an analysis of the most common materials which have been proposed. The quantity of information on Aluminum is far greater than that for any other type and for this reason analysis is performed in comparison to Aluminum. Figure 1-6 indicates that Magnesium and Magnesium Lithium alloy both requires less weight per unit area than Aluminum to stop penetration of a projectile with a given velocity. It is interesting to note from Figure 1-6 that Magnesium and Magnesium Lithium are significantly less dense than Aluminum. Due to the closeness of the three best bumper materials depicted in Figure 1-6 and the fact that far greater experience has been attained in working with Aluminum, design curves presented within this report will be on the basis of Aluminum 2219-T87. Relations from which design curves will be calculated will be presented so that any material may be analyzed, given the density, bar speed of sound, and Brinnel hardness.

Filament wound Fortisan fiber meteoroid shields and pressure vessel walls have been analyzed for their ability to prevent penetration by high velocity particles. Figure 1-8 more clearly illustrates the thicknesses and weights of a Fortisan Filament wound structure required to prevent penetration as compared to Aluminum and Magnesium Lithium. Designs depicted in Figure



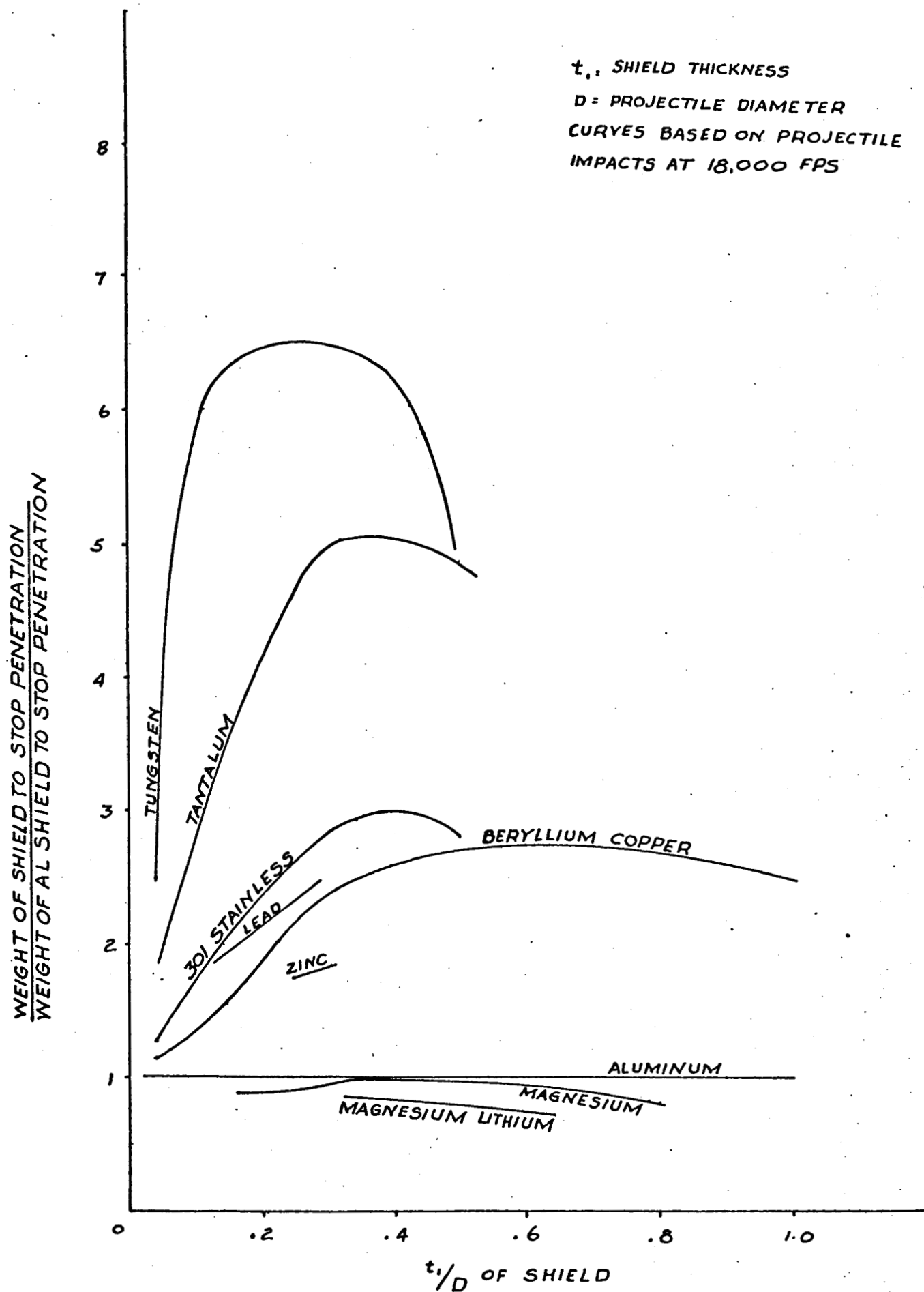


FIGURE 1-6 BUMPER MATERIAL BARRIER EFFICIENCY

Material	Density gm/cm <sup>3</sup>	Yield Strength ksi	Ultimate Strength ksi	Melting Temperature °F	Sonic Velocity fps	Modulus of Elasticity ksi	Specific Heat BTU/lb °F	Coefficient of Thermal Expansion in/in °F
Units								
Foamed Aluminum	1.2							$13.7 \times 10^{-6}$
2219-T6	2.77	37.3	55.8	930-1200	16,650	10.5	.22	$13 \times 10^{-6}$
2219-T87	2.77	50		930-1200	16,650	10.8	.22	$13 \times 10^{-6}$
2024-T3	2.77	50	70	935-1180	16,650	10.5	.22	$12.9 \times 10^{-6}$
2014-T3	2.77	61.5	69.1	950-1180	16,650	10.5	.22	$12.8 \times 10^{-6}$
Beryllium								
Copper	8.24	25-35	60-80	1600-1800	13,100	19	.10	$9.3 \times 10^{-6}$
AZ31B-H24								
Magnesium	1.74	32	42	1050-1170	15,700	6.5	.245	$16 \times 10^{-6}$
LA 141A								
Magnesium								
Lithium	1.35	15	19-25	1070	18,000	6	.346	$21.8 \times 10^{-6}$
TAM								
Molybdenum	10.2	105	125	4750	17,400	46	.061	$3.1 \times 10^{-6}$
Foamed Nickel	3.6- 2.52			2630				$9.2 \times 10^{-6}$

FIGURE 1-7 MATERIAL PROPERTIES

Material	Density gm/cm <sup>3</sup>	Yield Strength ksi	Ultimate Strength ksi	Melting Temperature °F	Sonic Velocity fps	Modulus of Elasticity fps	Specific Heat BTU/lb °F	Coefficient Of Thermal Expansion in/in °F
301 Stainless	7.84	40	110	2570	16,100	28	.12	$9.4 \times 10^{-6}$
321 Stainless	7.92	30	90	2570	16,100	28	.12	$9.5 \times 10^{-6}$
1095 Stainless	7.84	75-120	110-190		16,750	29-30	.10-.11	$8.1 \times 10^{-6}$
Tantalum	16.6	48	60	5425	11,000	27	.036	$3.6 \times 10^{-6}$
5AL-2.555 Titanium	4.73	137.8	142.9	2800-300	16,400	15-17.5	.135	$5.8 \times 10^{-6}$

FIGURE 1-7 (cont.) MATERIAL PROPERTIES

Material	Bumper		Hull		Adhesive wt. (lbs/ft <sup>2</sup> )	Foam weight (lbs.)	Total Weight lbs/ft <sup>2</sup>
	t (inches)	weight (lbs.)	t (inches)	weight (lbs.)			
2219-T87 Aluminum	*.018	0.26	.057	0.82	.17	.40	1.65
LA141A Magnesium- Lithium	*.020	0.14	.091	0.65	.17	.40	1.36
Fortisan Filament	.053	0.42	0.146	1.08	.17	.40	2.07

\*Corrugated

FIGURE 1-8 EXAMPLE - COMPOSITE METEOROID SHIELDS

1-8 are those required to prevent penetrations by particles traveling at the same velocity.

The author concludes and Reference 29 substantiates that the laminations of a fibrous bumper reduces its efficiency to prevent penetrations. Projectiles are not fragmented and penetrate relatively intact.

#### 4.2.1.1 CORRUGATED BUMPERS

Corrugated bumpers used in multiple-sheet meteoroid design are desirable in that they tend to turn impacting particles obliquely through the energy dissipating medium. The general consensus among investigators, including Reference (11), is that a hypervelocity particle will expend its energy normal to the impacting surface. Per reference (18), if 80% of the bumper surface offers an oblique surface a majority of the impacting meteoroids will be turned anywhere from 5° to 45° normal to the structure. In addition, energy is lost in the change in direction of the velocity vector.

Multiple splay impacts on corrugated targets, as observed in reference (18), resulted in part of the fragmented projectile skidding along the exterior surface of the corrugation cone. A portion of the fragmented projectile was able to penetrate the bumper resulting in elongated craters. It is estimated that a sine wave shaped bumper would increase the protection of a meteoroid bumper by a minimum of 20%.

#### 4.2.2 ENERGY ABSORBANTS FOR APPLICATION TO MULTIPLE-SHEET METEOROID SHIELDS

Many types of energy absorbing filler materials have been experimentally tested for their applicability to multiple-sheet meteoroid shields. They have included Polyurethane, Polystyrene, Q-felt, stabilized Q-felt, Dexiglas, Owens-Corning TW-F insulating Wool, and Armstrong low density Cork.

Early laboratory impact tests of composite structures have demonstrated the effectiveness of low density fillers in both reducing the total structural weight and increasing the total energy dissipating capability. However, per reference (29) it has been shown that under certain conditions particle impacts approaching meteoroid velocities can induce catastrophic failures.

Foil insulations consisting of close packed layers of foil laminates and closed cell foams are undesirable due to secondary damage effects. Upon impact the outer bumper shatters the projectile into many small particles some of which are vaporized, resulting in a highly compressed mass of material. When the fragmented material strikes an area of entrapped gas such as that found in closed cell foams and layers of foil, a pressure pulse is generated which shatters the filler material over a wide area adjacent to the projectile path. This pressure pulse substantially increases the damage to the rear pressure vessel wall. A similar effect has been observed by reference (29). The recommendation was made that a dead air space be provided between the shield and the main pressure vessel wall to relieve compressed gasses.

For the same density, fibrous filler material such as glasswool, and Q-felt is approximately as efficient as cellular material in dissipating energy. A difference is evident in the type of damage resulting for the reasons stated previously.

Figure 1-9 illustrated the effectiveness of glass wool to absorb energy at various velocities. It is significant to note the effect of providing an air space between the bumper and the filler material.

In addition to the sealed air problem relating to super-insulations employing foils, it has been experimentally determined by reference (29) that twice the weight of foil and insulation would be required to obtain the same stopping power offered by polystyrene foams.

To summarize energy absorbent analysis, the type of filler may be correlated to total main hull damage. Main hull or pressure vessel wall damage increases for the following materials in the order of listing.

- (1) Fiberglass wool with preceding air space
- (2) Fiberglass wool without preceding air space
- (3) Open cell foams
- (4) Closed cell foams
- (5) Low density cork
- (6) Super-insulations (foil layers)

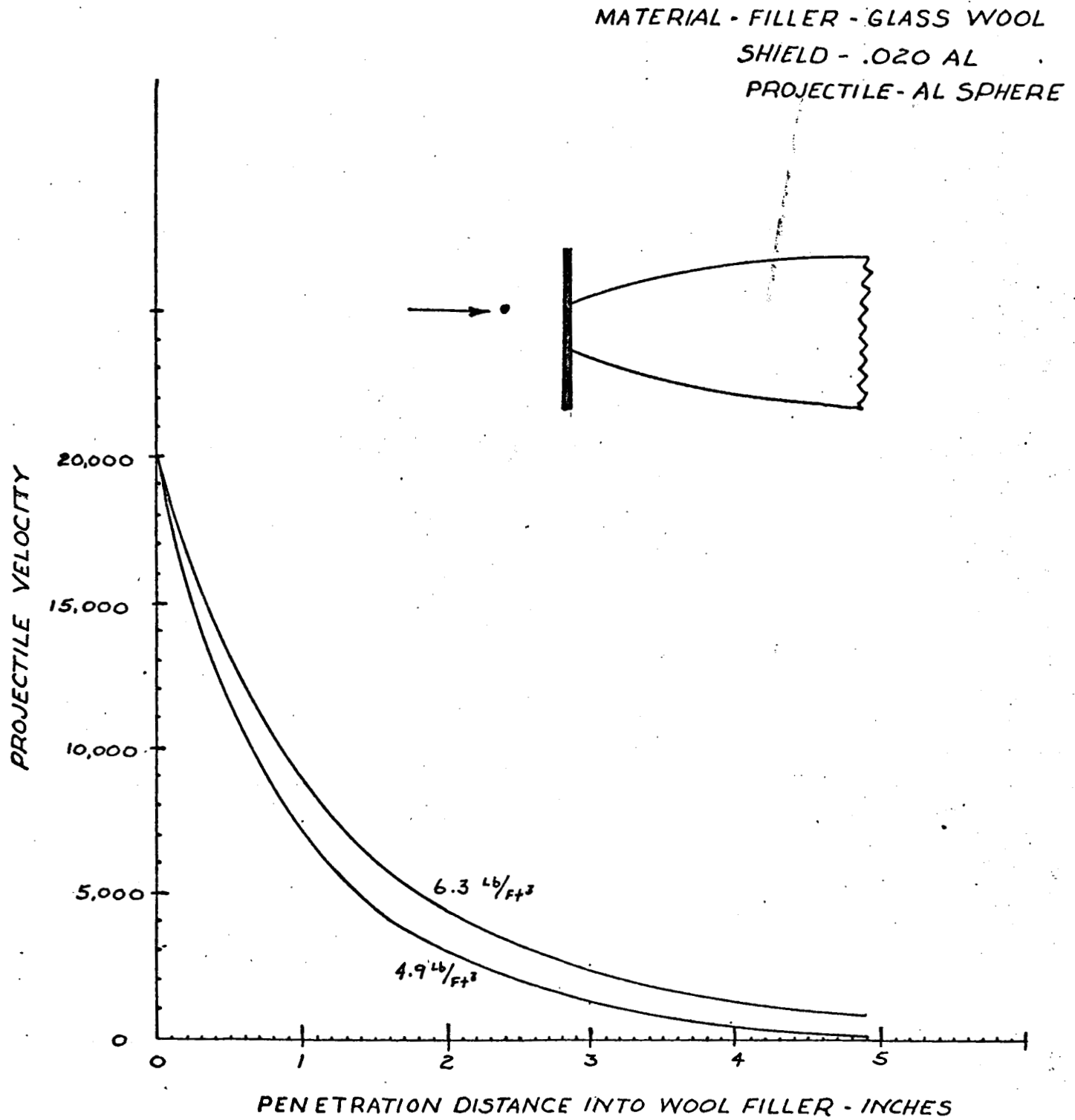


FIGURE 1- 9 GLASS-WOOL PENETRATION CHARACTERISTICS

MATERIAL - FILLER-GLASS WOOL  
 SHIELD - .020 AL  
 PROJECTILE - AL SPHERE

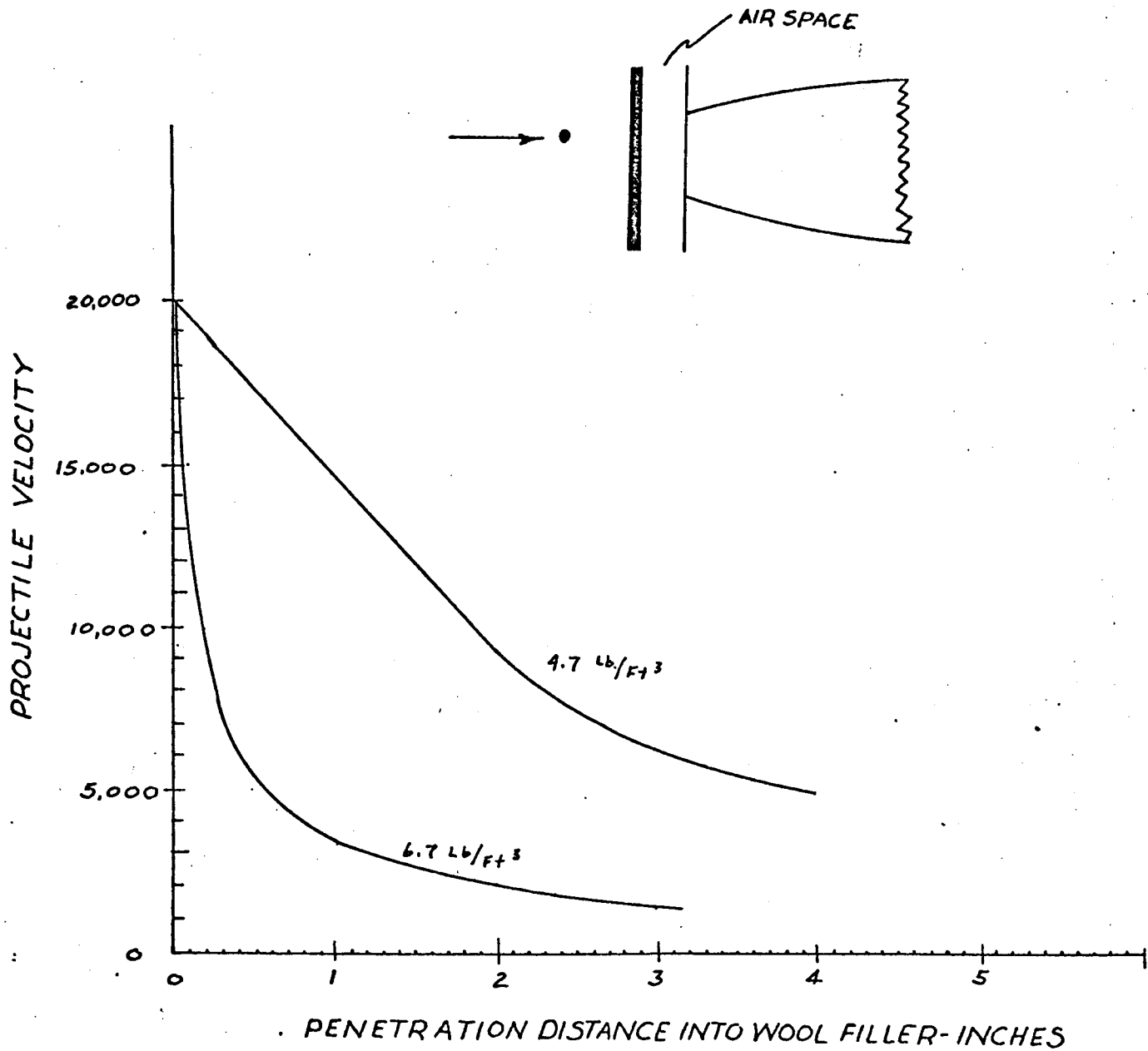


FIGURE 1-9 (cont.) GLASS-WOOL PENETRATION CHARACTERISTICS



Honeycomb applications to multiple-sheet meteoroid shields where the cellular structure runs perpendicular to the outer bumper contributes little to preventing penetration. Reference (29) found that while bumper damage was somewhat less adjacent to the point of impact, total penetration was about the same as for two sheets of Aluminum with no filler.

#### 4.3 REVIEW OF EXPERIMENTAL METHODS AND DATA

One of the most significant efforts to be performed in the area of meteoroid shielding design is the verification of specific designs in the hyper-velocity range. The multiple-sheet meteoroid shield design with various fillers applied have been validated in the 20 to 25,000 feet per second range and have previously been shown to be the best design up to this velocity.

##### 4.3.1 HYPER-VELOCITY EXPERIMENTATION

Per References (18, 28 and 31) the average meteoroid velocity is currently estimated to be 30 KM/sec (98,400 ft/sec). To validate multiple-sheet shielding in the range approaching meteoroid velocities reference (18) employed a particle accelerator capable of accelerations to 120,000 ft/sec.

Micrometeoroid accelerators capable of reaching particle velocities duplicating those to be found in space or on the lunar surface are limited in the size of particle which may be handled. Consequently, specific target designs to be used are theoretically scaled down to meet the maximum mass the test facility is able to fire. Conversely, using the same mathematical approach, the test results were treated to apply to the larger meteoroid particles to be actually found in the space and lunar environment. Experimentation in the hypervelocity range has not been accomplished without problems however. Listed below are significant results and difficulties which have been encountered in the accumulation of hypervelocity impact data. It must be noted that experimentation in this velocity range is new and it is not unreasonable to expect that the state-of-the-art may be such that a significant number of the problems may have been removed by the time that this study is released.

- (1) A high percentage of test particles were breaking up when accelerated above 30,000 ft/sec.

- (2) Procedures used to scale down meteoroid shielding designs to match particle sizes used in hypervelocity acceleration equipment is conservative.
- (3) At the present time equipment state-of-the-art is such that adequate equipment for monitoring particle integrity and velocities (60-200,000 ft/sec.) is not available.
- (4) It was anticipated that hypervelocity impact data such as that found in reference (18) would result in ballistic limit data for meteoroid shielding designs. However, of the references available, total penetrations of test panels were not obtained.
- (5) Due to item (4) above, test personnel in the hypervelocity range were not able to recommend changes to the generally accepted multiple-sheet meteoroid shielding designs. However, a typical approach, such as the NASA-AMES composite panel design procedure was shown to result in conservative designs.
- (6) Per reference (18), when considering the NASA-AMES composite panel design procedure; on the basis of hypervelocity test data, an 80% increase in mass over that for which designs were accomplished could be expected before the composite hull would be punctured.
- (7) Per references (18 and 28), the electric discharge accelerator (in development stages) offers the best prospects for particle accelerations from 100,000 to 200,000 ft/sec.

#### 4.3.2 STRESSED AND CRYOGENICALLY COOLED STRUCTURES

Significant weight reductions are realized for cryogenic modules in space applications by incorporating the propellant wall and insulation with the inner portion of the barrier. Meteoroid shielding designs applied in this manner to cryogenic modules will require that analysis be performed on the effects of fragment impact on stressed structures at cryogenic temperatures. It is generally anticipated that catastrophic failures will occur if internally stressed cryogenic tanks are penetrated

Tests have been performed by reference (29) on uniaxially and biaxially stressed cryogenic structures in the cooled and uncooled condition to determine the impact conditions necessary to induce catastrophic failure.

#### 4.3.3

#### SIGNIFICANT STUDIES

Reference 45 is a report of an investigation being performed for the Manned Spacecraft Center. The thoroughness with which the investigation is being performed and the results which have consequently been obtained justify a summary within the body of this report.

A basic deficiency in micrometeoroid impact simulation is the inability to reach true meteoroid velocities. The experimenters of reference 45 propose to understand the physics of impact so as to be able to extrapolate to hypervelocities. Listed below are some of the characteristics of the experimental procedure.

1. The meteoroid environment adopted for analysis is that identified in reference 37.
2. When specific meteoroid shielding panels are to be tested and the structural area, exposure period, and the zero puncture probability desired is known, the test particle size is determined by:
  - (a) calculating the meteoroid mass to be designed for
  - (b) calculating the particle diameter at .5 grams per cubic centimeter
  - (c) arriving at an equivalent aluminum particle diameter
3. The design criteria for establishing meteoroid shielding panels is minimum weight.

4. The meteoroid particle for which designs are established is denoted as the Apollo particle. It is established at .44 grams per cubic centimeter, travels at a mean velocity of 30.4 kilometers per second and is 1.02 millimeters in diameter.

## 4.3.3.1

The impact process      The following statements on impact physics are established:

1. At impact the projectile and meteoroid shield is shocked to some pressure.
2. The pressure generated at impact reduces to ambient pressure by release waves.
3. Pressure buildup and release cycle in the shield is nonisentropic. Consequently, heat is generated.
4. The heating generated at impact determines the debris particle size by the following:
  - (a) If the resultant debris is solid, the size of the particles will decrease with increasing temperature due to the decrease in fracture strength.
  - (b) If the resultant debris is molten, only surface tension forces need to be overcome to create droplets. These forces and correlating droplet sizes will become smaller as the liquid temperature increases up to the point where the debris is vaporized.

To further clarify the observations made above, the following statements refer to Figure 1-9A. However, it would be useful to first define the optimum meteoroid shield thickness. The optimum thickness ( $t_{opt}$ ) of a shield is that shield thick enough that the axial element of the shock reaching the back of the projectile is of sufficient strength to cause complete melting.

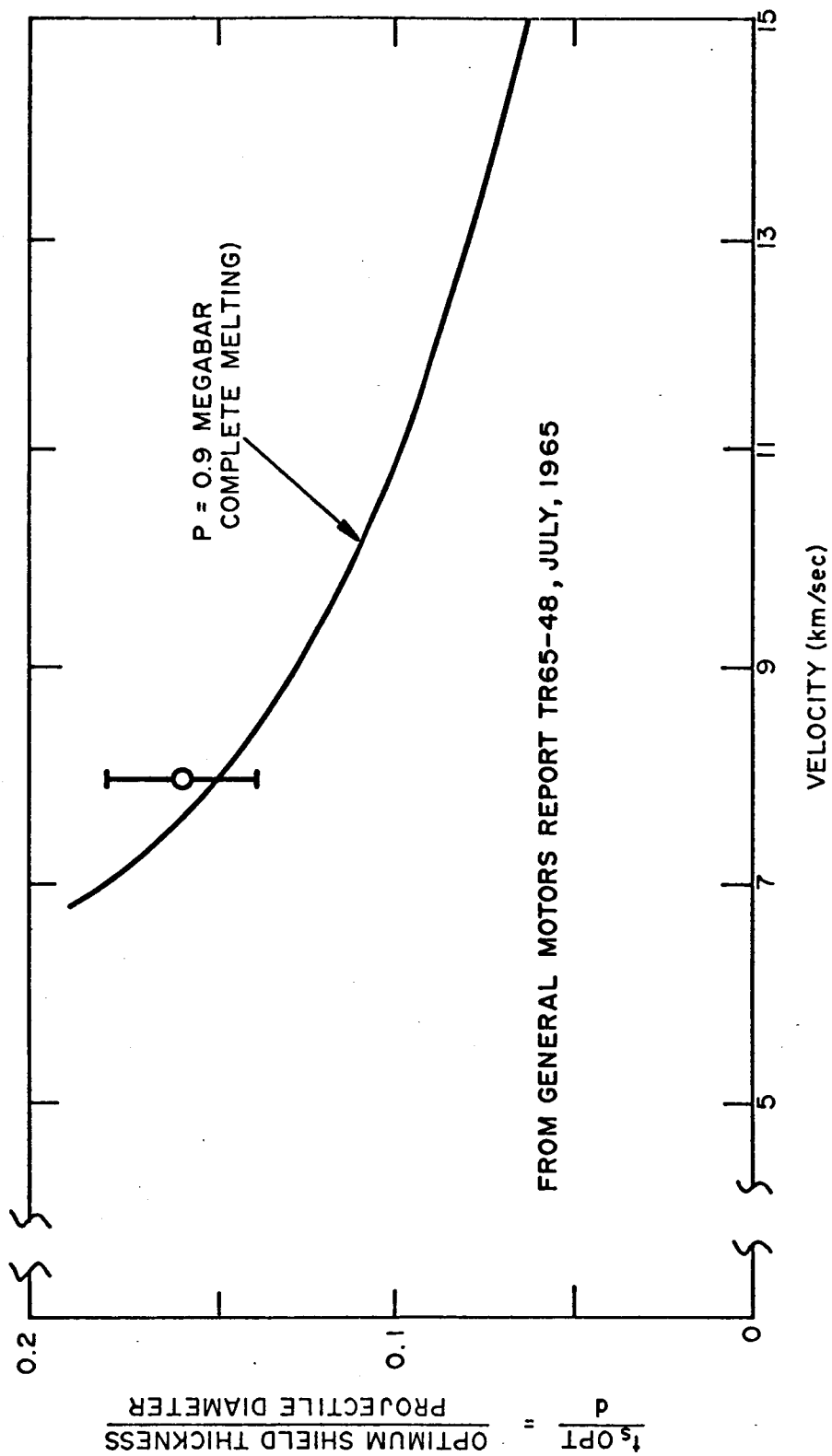


Figure 1-9A. OPTIMUM SHIELD THICKNESS — ALUMINUM SHIELD AND PROJECTILE

1. Note that the optimum sheet thickness is a function of impact velocity for aluminum shields and projectiles.
2. The theory works only for those velocities above that required to cause debris melting.
3. Optimum shield thickness ( $t_s$  opt) decreases with increasing impact velocity.
4. Density rather than the particular material is the design criteria.
5. The effectiveness of a shield is independent of the strength of the shield material at impact velocities above 4 kilometers per second.

Experimentation by the authors of reference 45 at 8.07 kilometers per second resulted in the following observations:

1. Most of the damage in a meteoroid shield does not occur across the full diameter of the resultant bubble at impact but instead over a central area with a diameter equal to approximately one-half of the diameter of the bubble.
2. Loading is uniform over the central damage area.
3. The main failure mode is tensile failure around the circumference of the loaded area. Failures were not initiated by shearing as was first thought by other experimenters.
4. Failure mechanisms were identified in two modes.
  - a. Formation of spallation
  - b. Failure in tension of which petalling is an indication.

5. The momentum transferred to the loaded area upon impact has been experimentally and theoretically determined to be twice the momentum of the original particle.

#### 4.3.3.2

#### Target Dynamic Deformation Analysis

The problem of determining dynamic deformations and stresses in thin shells involves a complex system of non-linear differential equations. A numerical technique has been developed to analyze large deflections and plasticity effects (witmer, et al). The technique involves a difference approximation for the original differential equations. These relations are then used to describe an equivalent lumped parametric model. All such calculations in Reference 45 to present use six incremental layers for computation purposes. Emphasis is placed on impact analysis and the physics of the procedure. A strip approximation method is applied to the impact analysis of the backup sheet.

Initial velocity  $V_i$  imparted to the central portion of a strip is given by:

Where;

$$v_i = \frac{32M_p V_p}{S^2 t_b \rho \epsilon_b}$$

Where  $M_p$  and  $V_p$  are the mass and velocity of the impacting particle :  $S$  is the spacing and  $\rho_b$  and  $t_b$  are the density and thickness of the backup sheet.

#### 4.3.3.3

#### Effect of Particle Size

It was determined that when back-up sheet thicknesses for yield and fracture criteria were plotted against particle diameter at a number of velocities,  $t_b$  (thickness of the back-up sheet) was approximately proportional to the cube of the particle diameter. Further,  $V_i$ , the initial velocity of the loaded area, is approximately constant.

#### 4.3.3.4 Sheet spacing

Sheet spacings investigated included 2.54, 5.08 and 10.16 centimeters at 30.4 km/sec for the Apollo particle. The Apollo particle is defined as the mean meteoroid presently established at .44 gm/cc density for a velocity of 30.4 km/sec.

A conclusion is that for each decrease in spacing (10.16 cm to 5.08 cm and 5.08 cm to 2.54 cm) the backup sheet thickness necessary decreases approximately with the inverse square of spacing. For 7075-T6 aluminum an appropriate equation for backup sheet thickness is given by:

$$t_b = C \frac{M_p V_p}{S^2}$$

where  $C = 415 \pm 140$  and  $82 \pm 14$  for the yield and fracture criteria, respectively

$t_b$  - thickness of the backup sheet in millimeters

$M_p$  - particle mass in grams

$V_p$  - particle velocity in km/sec

$S_1$  - spacing in centimeters

#### 4.3.3.5 Effect of Pre-tensioning the Backup Sheet

Frequently, space structures will include pressurized structures to be protected from the meteoroid environment. An analysis was run by both General Motors and Boeing and in general reach the same conclusions. General Motors obtained solutions for the Apollo particle with pre-tensioning of 25%, 50%, 75%, and 100% static yield stresses. When centerline displacements are plotted against time, (see Figure 1-9B) the indications are that pre-tensioning can significantly decrease the deflection of the backup sheet. However, the backup sheet thicknesses required for both the yield and fracture criteria are different. A conclusion is that the thickness required for



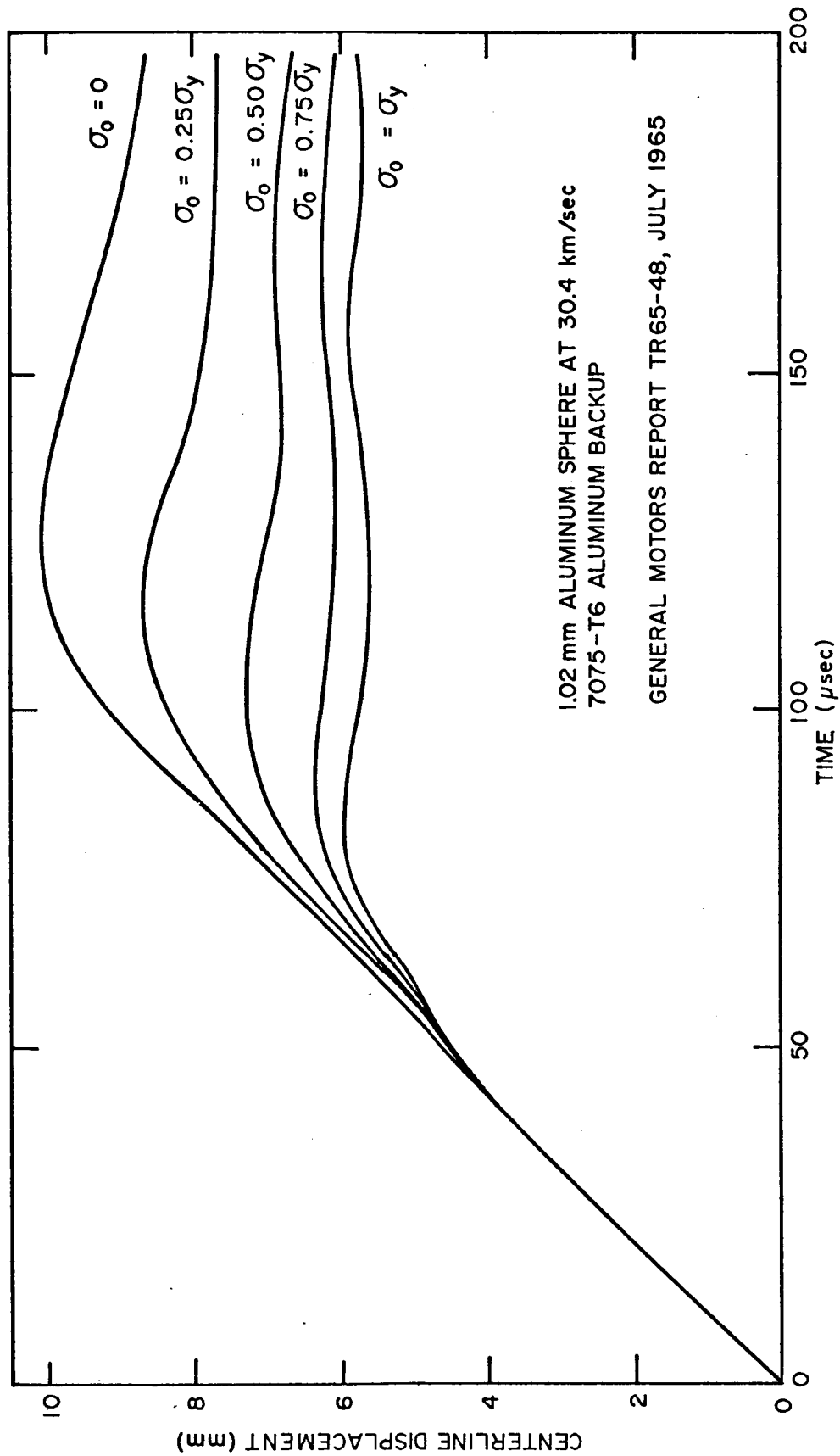


Figure 1-9B. PRE-TENSIONED BEAM BEHAVIOR - CENTERLINE DISPLACEMENT VS TIME

the yield criterion is not very sensitive to pre-tension, whereas the thickness based on the fracture criterion is sensitive to the amount of pre-tension. (See Figure 1-9C).

#### 4.3.3.6 Momentum Multiplication

An experimental analysis was performed in the area of momentum multiplication by General Motors. Momentum multiplication is the ratio of the measured momentum applied to the backup shield divided by the incident momentum. Significant conclusions are as follows:

1. The momentum multiplication factor for thin-sheet impacts was found to have an upper bound of 2.0.
2. With thicker shields, the momentum multiplication factor will show an increase.
3. Thin shields were identified as falling within the range of .305 to 1.02 millimeters.
4. It was concluded from experimental observations that bumper spacing has no effect on momentum transfer.

#### 4.3.3.7 Multiple Backup Sheets in Meteoroid Shielding Structures

Experimental results indicate that the use of multiple backup sheets offers little or no advantage over single backup sheets, as there is no significant decrease in the momentum through the second sheet until it has a thickness of approximately 90% of the fracture thickness.

All experimental tests were run on a momentum pendulum. In some cases where an analysis of the effect of the Apollo particle was desired, different size projectiles were used. When this was done a trade-off between particle diameter and velocity was accomplished to make the momentum equal to that of the Apollo particle. The Apollo particle was identified as being 1.02 mm in diameter and traveled at 30.4 km/sec.

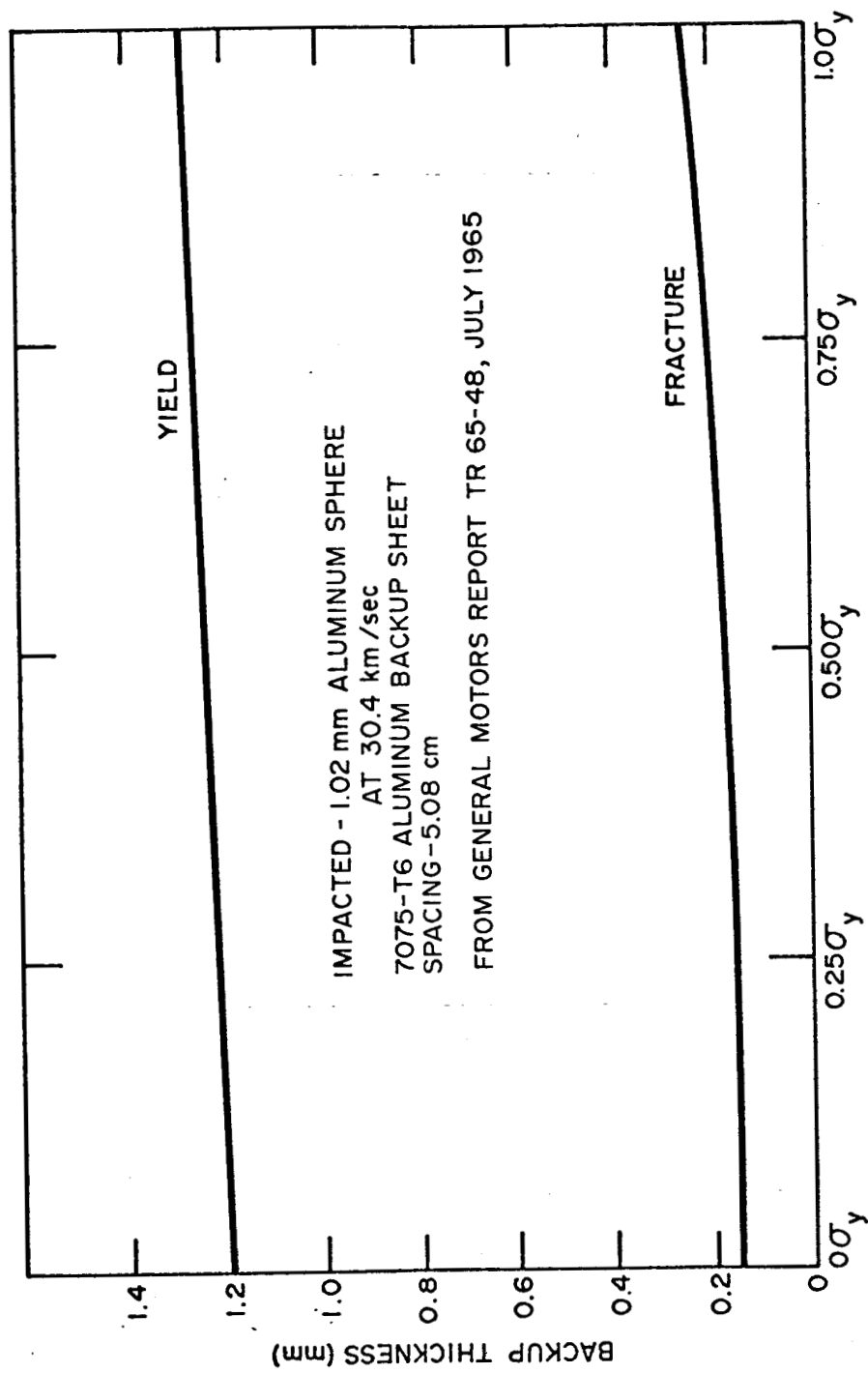


Figure 1-9C. PRE-TENSIONED BEAM BEHAVIOR - BACKUP THICKNESS VS. PRE-TENSIONED STRESS

## 4.3.3.8

Meteoroid Shield Determination

The procedure to be used for the establishment of an optimum meteoroid shield is summarized below.

1. Determine the critical meteoroid mass from an appropriate flux equation given the structural area, mission duration, and zero puncture probability desired. Apollo particle is the same as a 1.02 millimeter diameter aluminum sphere.
2. From Figure 1-9A we see that for the Apollo particle a .20 millimeter aluminum shield ( $T_s/d = 0.19$ ) will be adequate at velocities above 7 kilometers per second.
3. From Figure 1-9D we see that for a spacing of 5.08 centimeters and a velocity of 30 kilometers per second, a 1.20 millimeter backup sheet of 7075-T6 aluminum is not expected to yield.
4. The final design check is to see if the structure will resist penetration at velocities below 7 kilometers per second. From Figure 1-9E we see that a maximum backup thickness of 1.30 millimeter ( $t_b/d = 1.25$ ) is required at a velocity of 3 kilometers per second. Consequently, for this particular Apollo mission, the required total thickness of the meteoroid shield must be 1.50 millimeters.

## 4.4

MICROMETEOROID PARTICLE CHARACTERISTICS

Meteoroid particle density is generally agreed upon as being 0.44 grams per cubic centimeter and was first estimated by Whipple in reference (31).

For purposes of analysis to be accomplished within this report, a mean velocity of 30 kilometers per second (98,400 feet per second) is assumed. (See reference (30).)

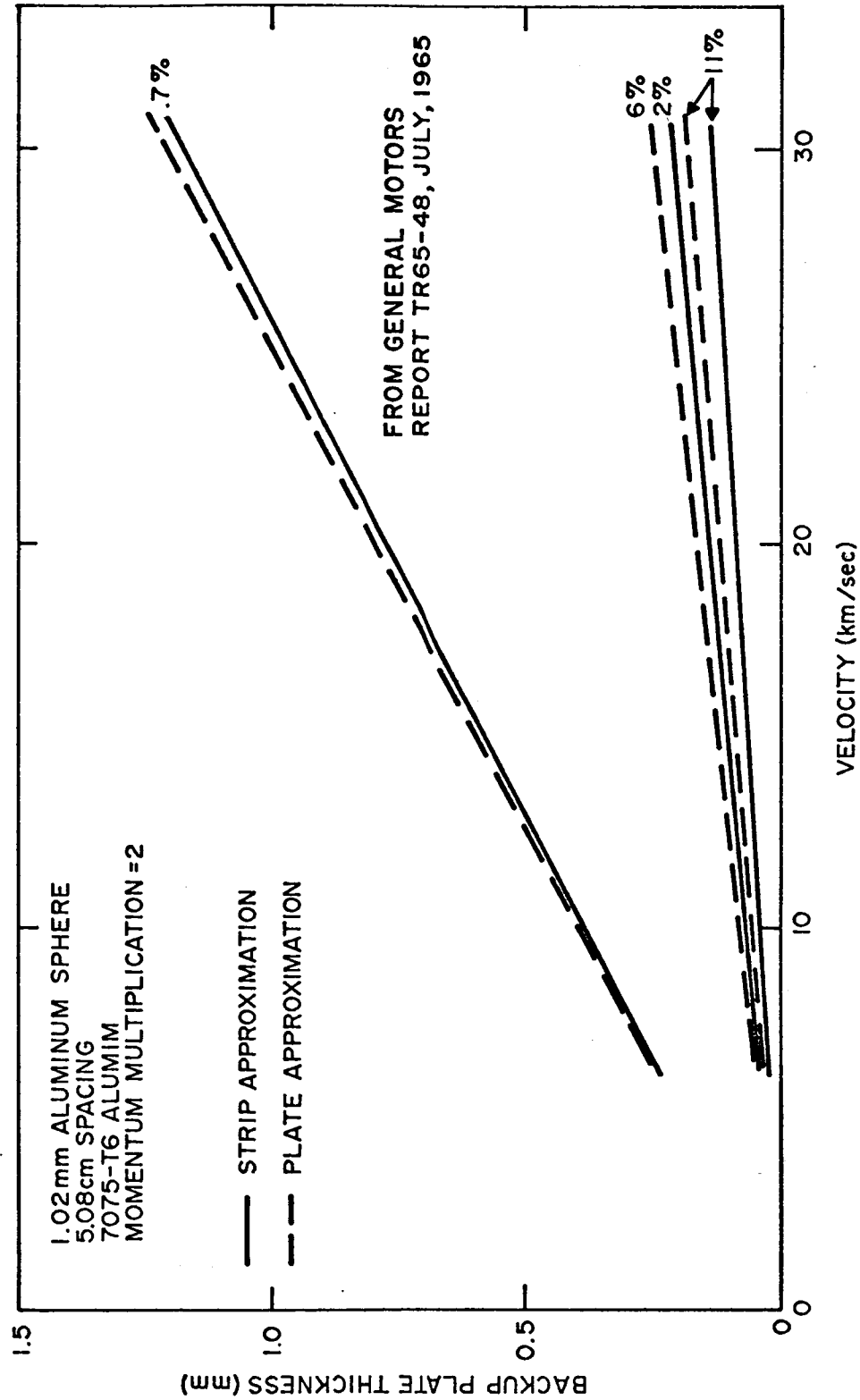


Figure 1-9D. COMPARISON OF STRIP AND PLATE CALCULATIONS - APOLLO PARTICLE

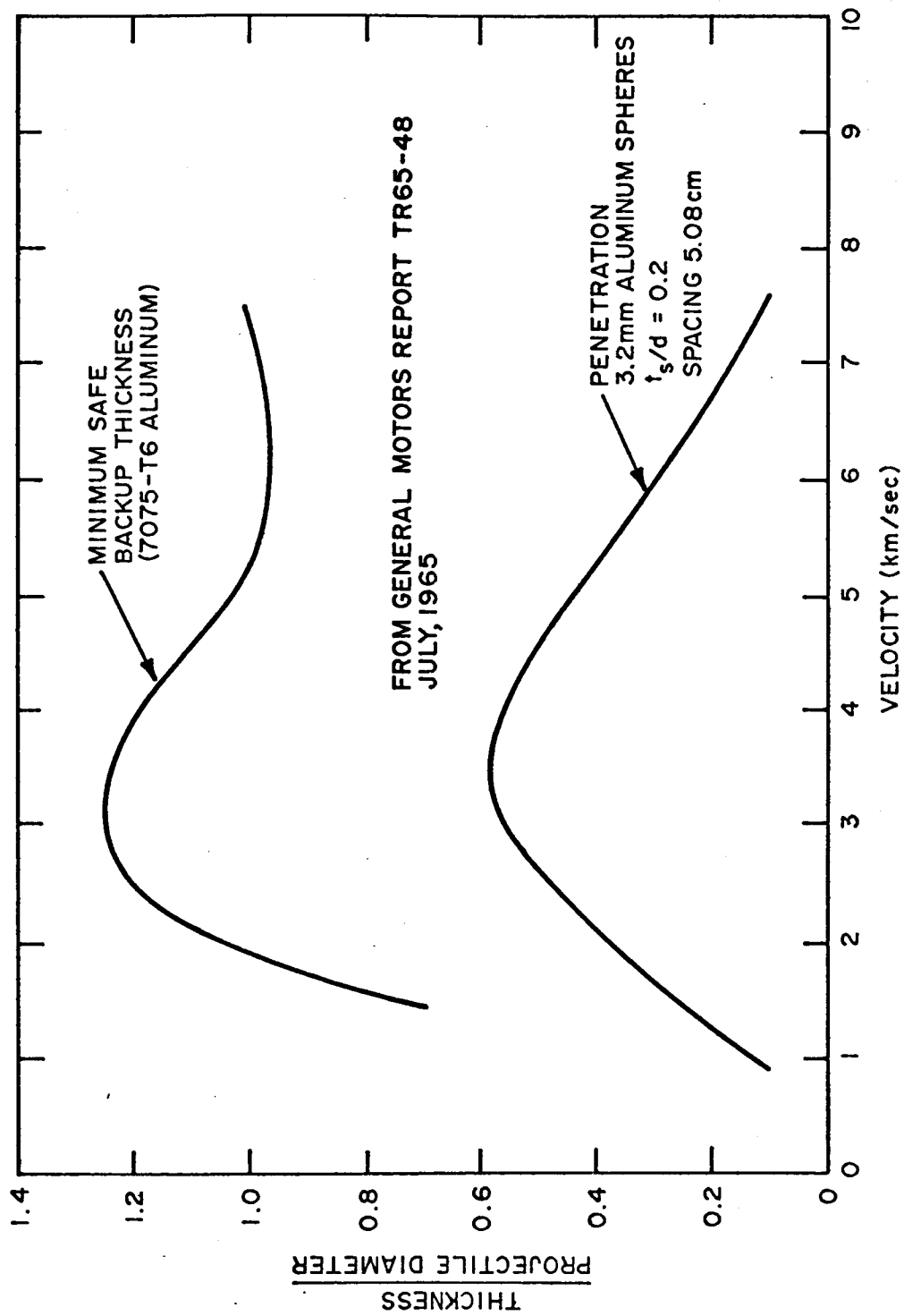


Figure 1-9E. BACKUP THICKNESS NECESSARY TO PREVENT PENETRATION

Significant flux and penetration data is anticipated from the Pegasus experiment now in orbit. The Pegasus payload employs three different aluminum sheet thicknesses for flux and penetration analysis (see Figure 1-10). For purposes of discussion here we will call them thin, thick, and thicker. The thin plate is constructed of .0015 inch soft aluminum 1100-H14 and offers  $8.256 \text{ m}^2$  (88.867 square feet) surface area. Reference (30) predicts 5,430 punctures for a one year period following orbit injection. The thick plate is constructed of .008 in. 2024-T3 hard aluminum and offers  $17.544 \text{ m}^2$  (188.842 square feet) of exposed surface. Reference (30) predicts 41 punctures for the one year period. The thicker plate of the three used is made up of .016 inch 2024-T3 hard aluminum with  $188.856 \text{ m}^2$  (2032.829 square feet) exposed surface. Thirty-eight punctures are anticipated for the first year of operation. This later portion of the Pegasus experiment is being followed with interest as the sheet thickness and exposure area approximates that of anticipated space and lunar structures. The estimated mass of the meteoroid particle which is capable of penetrating .016 inch 2024-T3 aluminum at 26.7 Km/sec is computed at  $10.47 \times 10^{-6}$  grams. Assuming a mean meteoroid density of .44 grams per cubic centimeter the particle is computed to be  $2.3 \times 10^{-5}$  cubic centimeters in volume or approximately .035 centimeters in diameter.

Per reference (32) it is of interest to note than when various configurations of lunar structures were considered, the maximum exposed area was  $597.9 \text{ ft}^2$ . If the projected puncture estimation of the thicker plate is shown to be accurate this structure could expect approximately 11.2 punctures per year or .93 punctures per month.

Material	Number of Panels	Exposed Area .516 m <sup>2</sup> /Panel	Panel Thickness (Inches)	Estimated No. of Punc- tures(1st Yr)	Meteoroid Mass (Grams)	Meteoroid Volume (Cubic Centimeters)	Meteoroid Particle Diameter (Centimeters)
1100-H14 Soft Al.	16	8.256 M <sup>2</sup> (88.867Ft <sup>2</sup> )	.0015	5430	-7.84 10 (14.45 x 10 <sup>-9</sup> )	3.3 x 10 <sup>-8</sup>	.004
2024-T3 Hard Al.	34	17.544M <sup>2</sup> (188.842Ft <sup>2</sup> )	.008	41	-5.85 10 (14.13 x 10 <sup>-7</sup> )	3.2 x 10 <sup>-6</sup>	.018
2024-T3 Hard Al.	366	188.856M <sup>2</sup> (2032.829Ft <sup>2</sup> )	.016	38	-4.98 10 (10.47 x 10 <sup>-6</sup> )	2.3 x 10 <sup>-5</sup>	.035

FIGURE 1-10 PEGASUS EXPERIMENT - METEOROID PUNCTURE ANALYSIS



#### 4.5 THEORETICAL METEOROID FLUX AND PENETRATION MODEL

Treatment of the primary meteoroid flux environment is separated into two general areas of interest, that applicable for the near earth - cislunar and lunar orbit - lunar surface environments. In addition to a treatment of the primary meteoroid flux for the lunar surface it has been determined that the lunar secondary flux imposes a significant hazard to lunar structures. Consequently, it will be handled in a manner similar to the primary meteoroid flux for the purposes of defining a meteoroid shielding design criteria.

It is necessary to differentiate between the primary meteoroid flux found near the earth and moon to account for inherent differences. It has been estimated by the author of reference (33) and (34) that the flux of primary meteoroids near the moon with mass equal to or greater than one gram is 40 percent of the corresponding near-earth value. This is generally substantiated by the author of reference (35). Although meteoroids considerably larger than one gram were considered it was thought that the flux of the larger meteoroids was 1/2 of that near the earth.

For purposes of simplifying the presentation leading to a convenient method of designing a meteoroid shield, the lunar flux and correlating penetration model are presented together. Resultant designs consist of a homogeneous single sheet structure. The method of transfer from a homogeneous meteoroid shield to a equivalent effective multiple sheet structure is presented in another section.

##### 4.5.1 NEAR-EARTH AND CISLUNAR METEOROID FLUX AND PUNCTURE MODEL

The following models are listed and discussed in detail in reference 44.

###### (a) Cumulative impact flux on a total sphere

$$F_s = 10^{-14.54 \pm 0.60} m^{\beta_2}$$

where

$F_s$  = the mean number of primary impacts per square meter of the exposed structure per second with mass equal to or greater than  $m$  grams ( see figure 1-11)

$$\beta_2 = - \left[ 1.00 + (0.34) \left( \frac{h}{100} \right)^{0.113} - 0.24 \log \left( \frac{h}{100} \right) \right]$$

$h$  = height in kilometers above the earth

assuming

$$\log \rho = \overline{\log \rho} = \pm 0.30 \text{ (i. e., } \overline{\log \rho} = (\log 0.44) \pm 0.30 = \text{meteoroid gravity specific)}$$

$$\log V = \log 19.4 \pm 0.12 = \text{meteoroid velocity in kilometers/second.}$$

Solving for  $\beta_2$  for a 200 nautical mile orbit we obtain the following:

$$200 \text{ nautical miles} = 370.65 \text{ kilometers}$$

$$\beta_2 = - \left[ 1.00 + (0.34) \left( \frac{370.65}{100} \right)^{0.113} - 0.24 \log \left( \frac{370.65}{100} \right) \right]$$

$$\beta_2 = -1.257$$

For a 200 nautical mile orbit our flux equation becomes

$$F_s = 10^{-14.54 \pm 0.60} \bar{m}^{-1.257}$$

(b) Puncture Flux

$$\phi = 10^{-13.84} \bar{m}^{\beta_2}$$

where

$\bar{m}$  = mass in grams of a nominally puncturing meteoroid.

$$\bar{m} = 10^{11.193 \pm 0.45} (PC_t^{0.50} E_t^{1.31} V_t^{8.0} \epsilon_t^{0.43})^3$$

$\phi$  = number of punctures of a randomly oriented vehicle per square meter of exposed area per second.

and

$p$  = thickness of a homogeneous metallic wall in centimeters

$C_t$  = Bulk Velocity of sound in kilometers per second

$E_t = 10^{-6}$  times Young's modulus in kilograms per square centimeter

$\epsilon_t$  = ductility (percent elongation in 2-inch gauge length at fracture)

$V_t$  = Poisson's ratio

For a 200 nautical orbit our puncture flux equation becomes.

$$\phi = 10^{-13.84} m^{-1.257}$$

where

$$m = 10^{11.193 \pm 0.45} (P C_t^{0.50} E_t^{1.31} V_t^{8.0} \epsilon_t^{0.43})^3$$

The following derivation is made to arrive at a single equation which may be used to determine the skin thickness required to prevent puncture of a structure with a set statistical zero puncture probability, and with surface area A for a mission duration t.

$$\bar{N} = \phi At$$

where

$\bar{N}$  = the average number of punctures of particles with mass equal to or greater than m grams, through the skin of a structure with surface A square meters during a period t seconds long. Orbital altitude is assumed at 200 nautical miles.

$$\bar{N} = \phi At = At 10^{-13.84} m^{-1.257}$$

For the probability of occurrence of a specified number of penetrations per unit of time, an accepted method of approach employs the mathematical Poisson model. In terms of the average number of penetrations  $\bar{N}$  on a given structure the probability p(N) of N penetrations is:

$$p(N) = \frac{1}{N!} \left[ (\bar{N})^N e^{-\bar{N}} \right]$$

Setting the requirement for zero penetration we get:

$$P(0) = e^{-\bar{N}}$$

or

$$\log_e P(0) = -\bar{N}$$

Substituting in our penetration flux equation for the average number of penetrations for a given structure in a 200 nautical orbit we get:

$$-\log_e P(0) = At 10^{-13.84} m^{-1.257}$$

where:

$$m = 10^{11.193 \pm 0.45} (P C_t^{0.50} E_t^{1.31} V_t^{8.0} \epsilon_t^{0.43})^3$$

For Aluminum 2219-T87

$$C_t = 5.075 \text{ kilometers/sec.}$$

$$E_t = .745 \text{ kilograms/cm}^2$$

$$V_t = .325$$

$$\epsilon_t = 5\%$$

Hence for Aluminum 2219-T87 the meteoroid mass required to penetrate a thickness  $P$  centimeters is as follows:

$$\begin{aligned} m &= 10^{11.193 \pm 0.45} (p \cdot 5.075^{0.50} \cdot .745^{1.31} \cdot .325^{8.0} \cdot .05^{0.43})^3 \\ &= 10^{11.193 \pm 0.45} (p^3 \cdot .0143 \times 10^{-11}) \end{aligned}$$

For a 75% confidence level  $\pm 0.45 \rightarrow -0.45$ . For a 50% confidence level  $\pm 0.45 \rightarrow 0$ . The latter will be treated first.

$$m = 10^{11.193} (.0143 \times 10^{-11} p^3) = .0223 p^3$$

Our penetration flux equation now becomes:

$$\begin{aligned} -\log_e p(o) &= At \cdot 10^{-13.84} (.0223 p^3)^{-1.257} \\ p &= -7.6 \times 10^{-4} \left[ \frac{At}{\log_e P(o)} \right]^{.2652} \end{aligned}$$

Where  $p$  represents the single sheet homogeneous wall thickness in centimeters of Al 2219-T87 required to prevent penetration of a structure  $A$  square meters in area, for a mission duration of  $t$  seconds, at a no puncture probability level of  $P(o)$ . The confidence level is established at 50 percent i.e., numerically speaking there is an even chance that the true values will fall to either side of that from the prescribed equation. Figure 1-12 presents design curves for zero puncture probabilities of .90, .95, .990, .995 and .999.

The following constitutes treatment of our original equation to provide a 75 percent confidence level.

$$m = 10^{11.193 - 0.45} (p^3 \cdot .0143 \times 10^{-11})$$

$$m = .00791 p^3$$

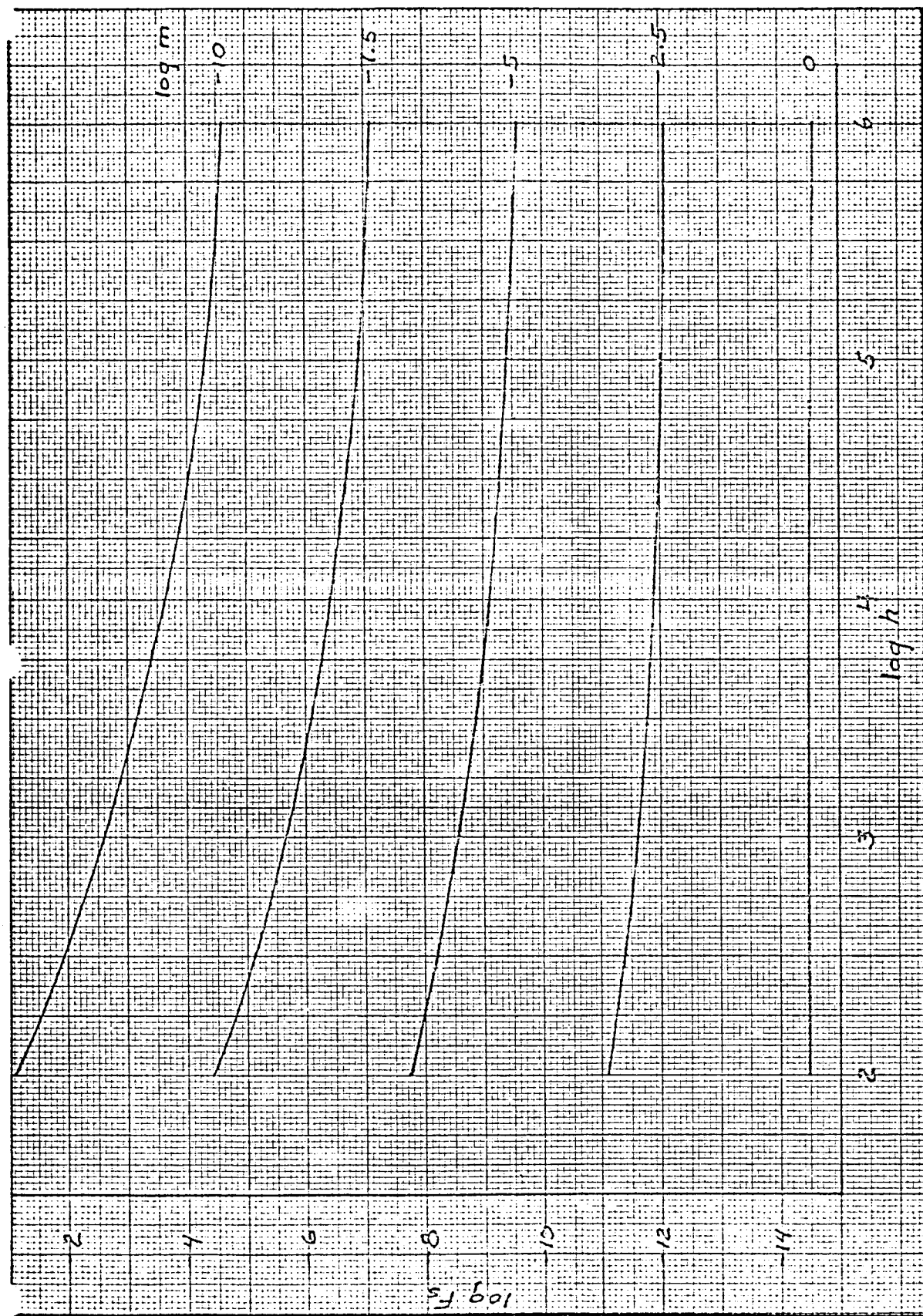
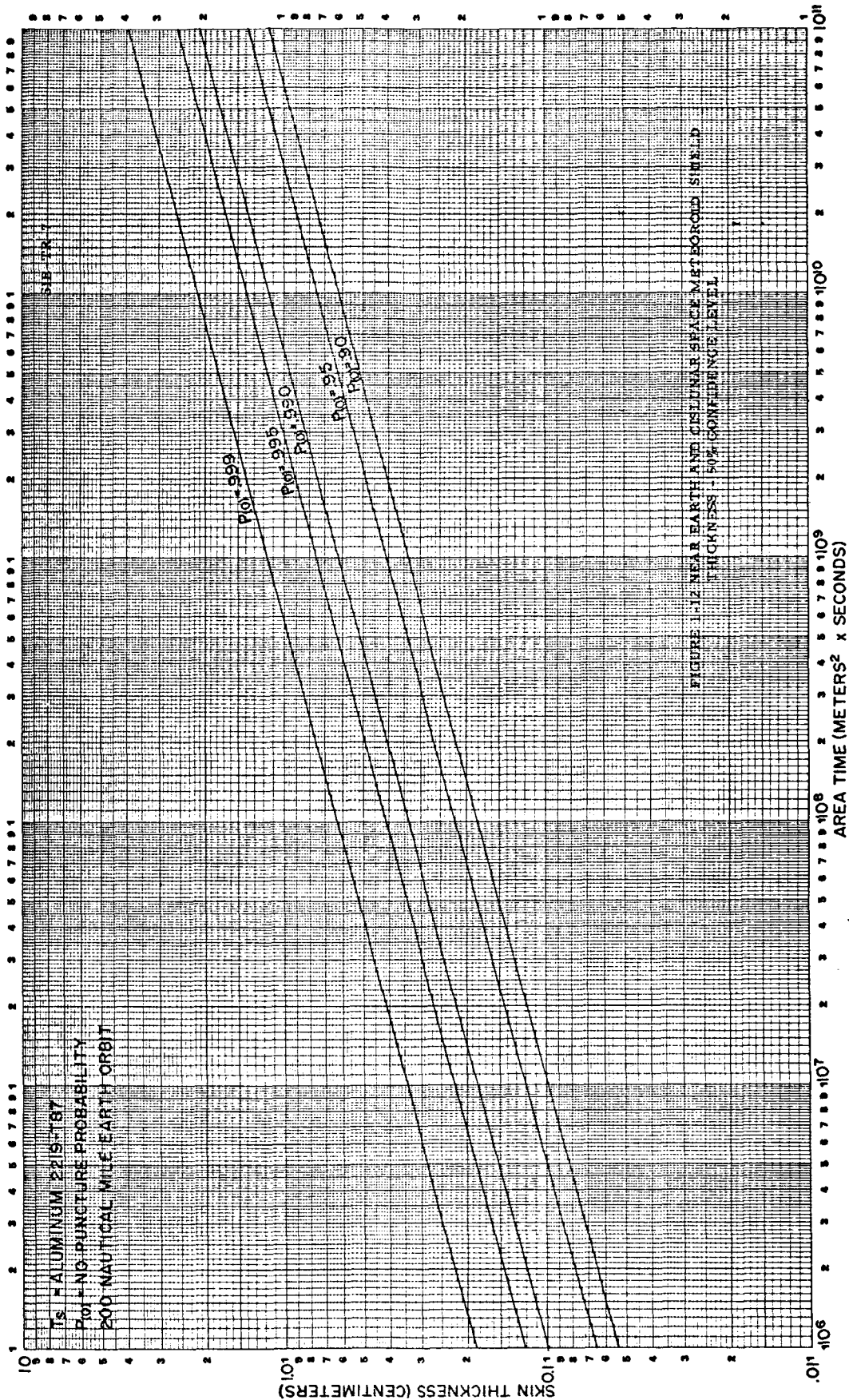
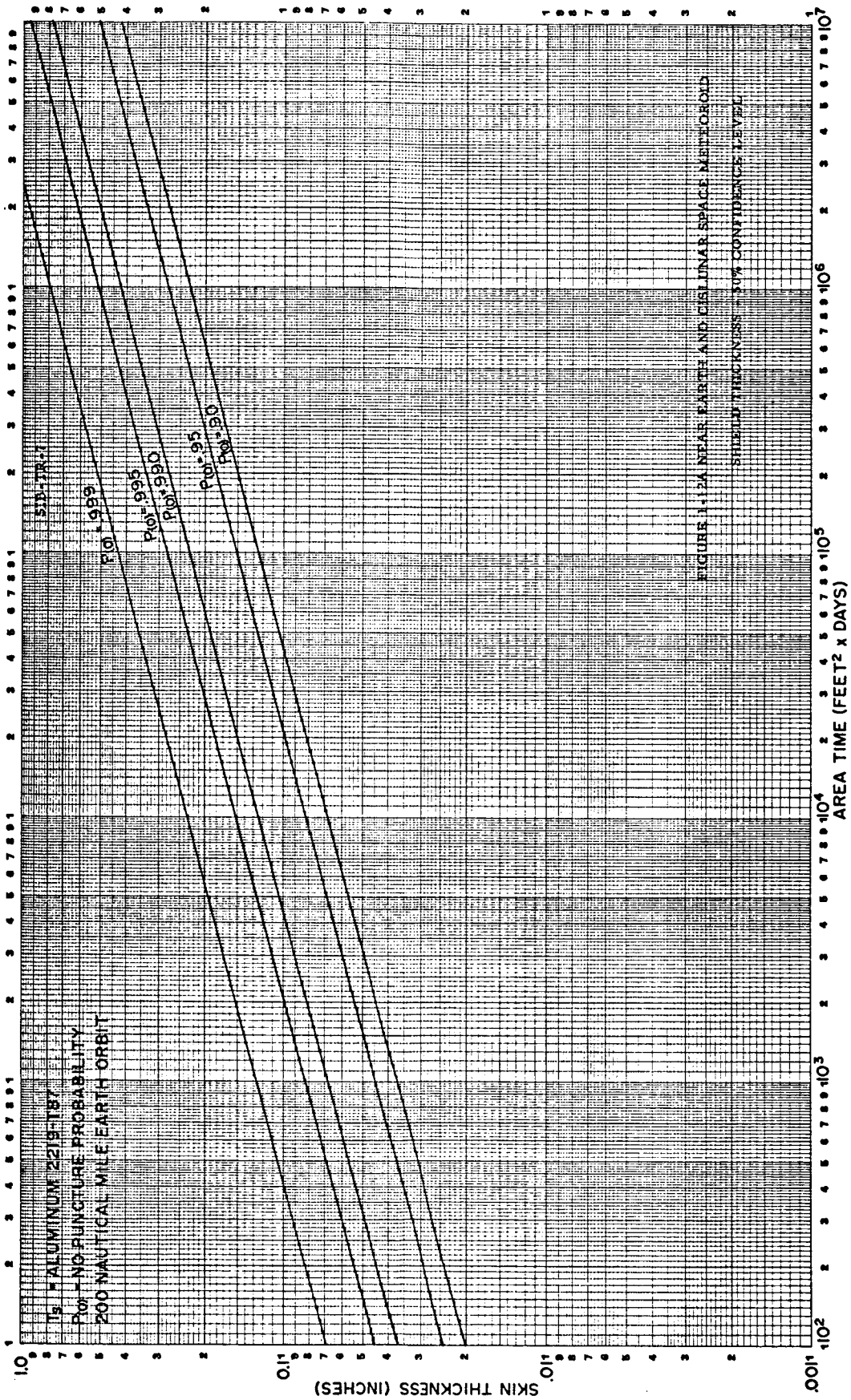


FIGURE 1-11 FLUX  $F_s$  WITH MASS EQUAL TO OR GREATER THAN  $m$  GRAMS AT  $h$  KILOMETERS ABOVE THE EARTH





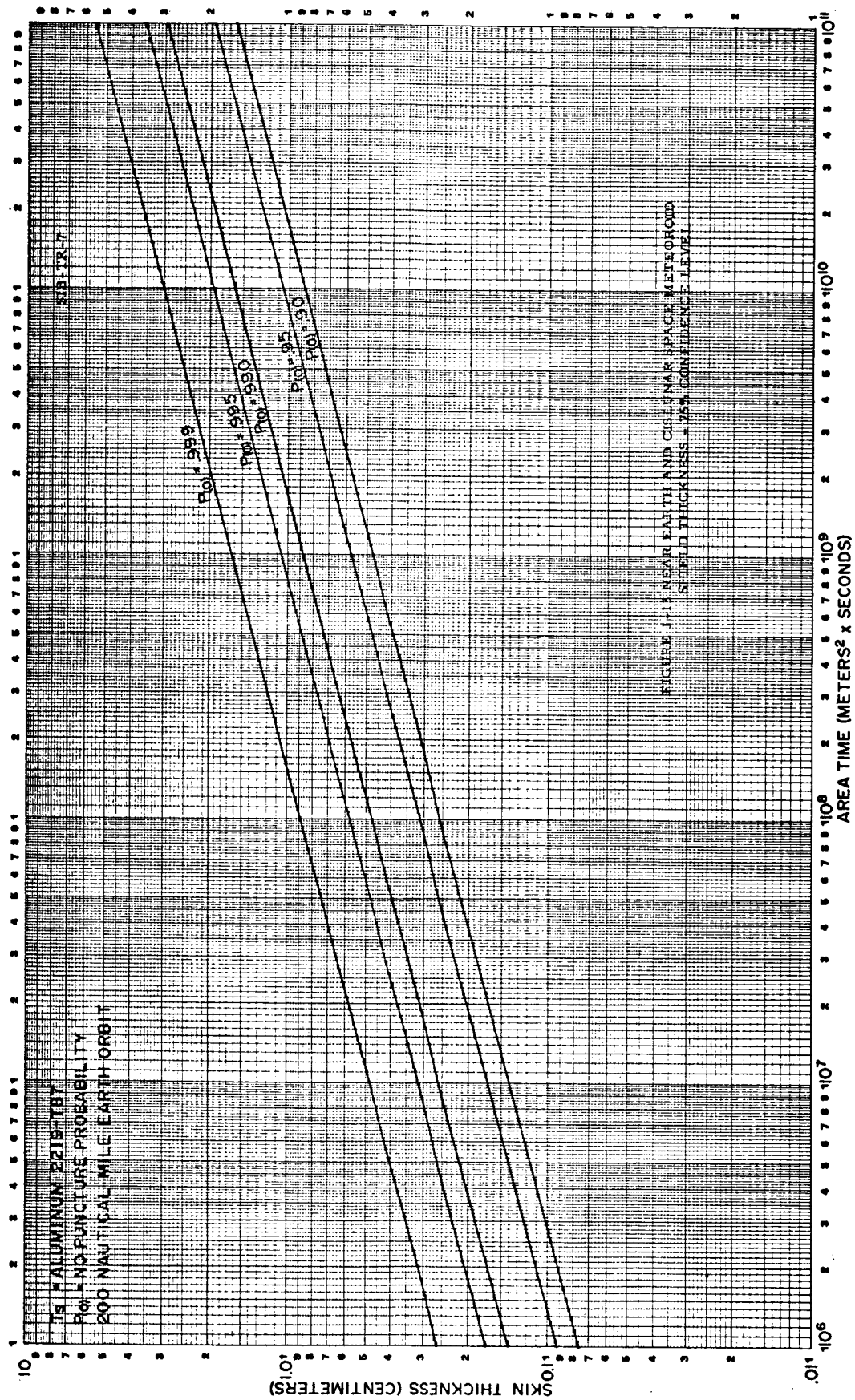
Our penetration flux equation now becomes

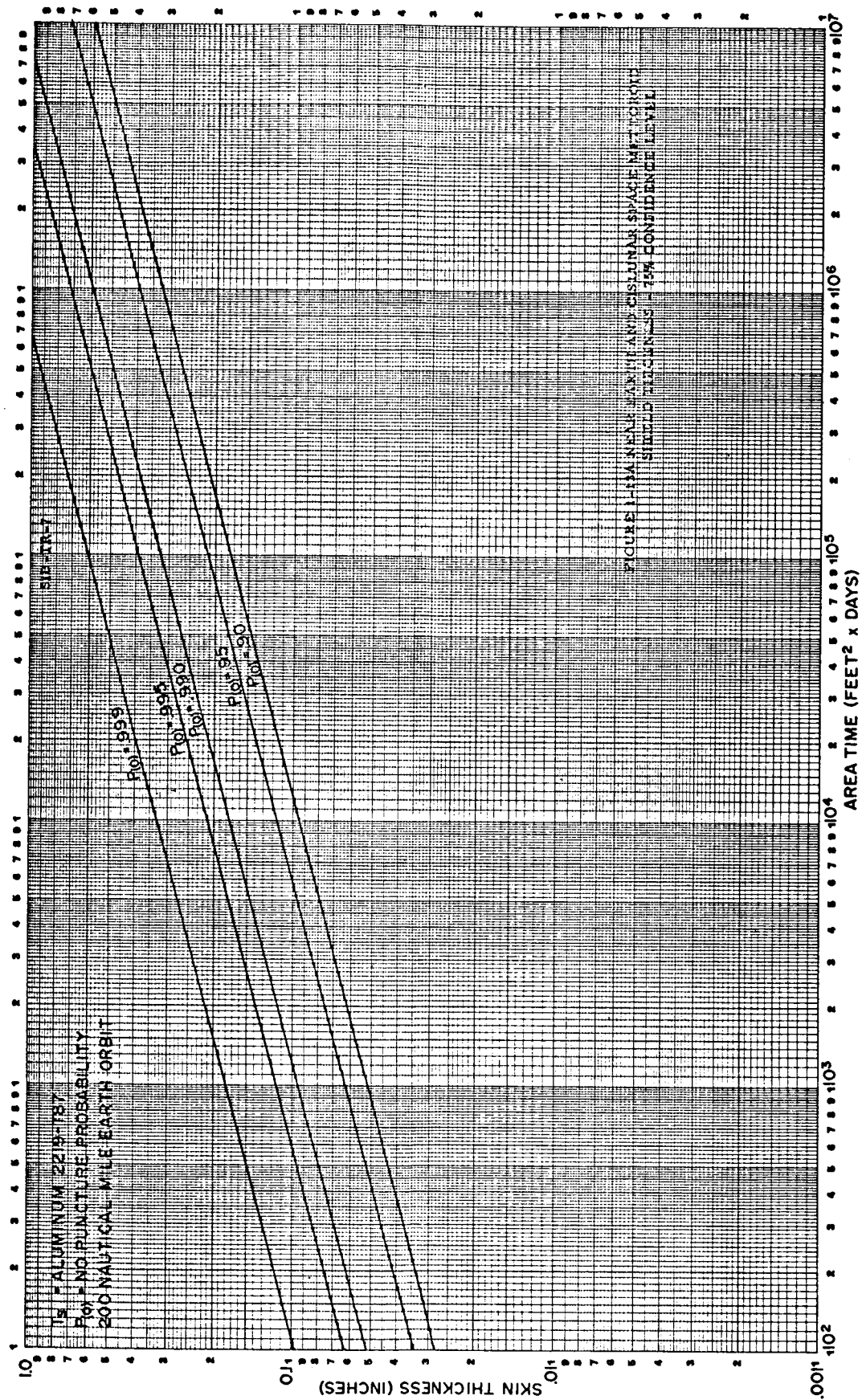
$$\begin{aligned}
 -\log_e P(o) &= At 10^{-13.84} (.00791 p^3)^{-1.257} \\
 p^{3.771} &= - \left[ \frac{At}{\log_e P(o)} \right]^{.2652} (.0636 \times 10^{-10})^{.2652} \\
 p &= -10.72 \times 10^{-4} \left[ \frac{At}{\log_e P(o)} \right]^{.2652}
 \end{aligned}$$

Where p represents the single sheet homogeneous wall thickness in centimeters of Al 2219-T87 required to prevent penetration of a structure A square meters in area for a mission duration t seconds, at a no puncture probability of P(o). Confidence level is established at 75 percent.

Figure 1-13 presents design curves for zero puncture probabilities of .90, .95, .990, .995 and .999.







#### 4.5.2 LUNAR SECONDARY PROJECTILE FLUX AND PUNCTURE MODEL

Fragments ejected from the lunar surface by primary meteoroid impact have been analyzed theoretically. These results duplicated experimentally indicate a substantial potential hazard to lunar structures. It is predicted that the flux of fragments of a given mass which are ejected from the lunar surface is at least  $10^3$  and possible  $10^4$  times greater than the flux of primary particles of the same size. (Reference 38) Although velocities are expected to be lower, average particle mass will be higher. The resultant effects on meteoroid shielding design, both homogeneous and multiple-sheet is presented in another section of this report.

While impact physics at hypervelocities is thought to be reasonably well understood, some concern has been recently expressed over the knowledge attained in the low velocity ranges. Several experimenters and theoreticians including those of references 30, 37, and 45 have indicated that penetration of common meteoroid shielding at low velocities may be substantially more severe than was first thought.

The following is adopted as the basic flux model for lunar secondary particles (Reference 37) and is adapted by the author to an appropriate penetration criteria. The procedure is construed to represent an acceptable method to establish homogeneous single sheet shields until such time that better data is available on low velocity impact physics. A method of transfer from single sheet designs to specific equivalent effective multiple sheet structures is presented in another section.

$$\log F_s = -1.34 \log m - 6.59$$

where:

$F_s$  The mean number of secondary impacts per square foot of the effected structure surface per day with mass equal to or greater than  $m$  grams.

The relation stated above accepts the following preconditions:

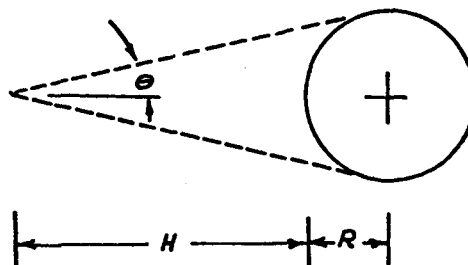
mean secondary particle velocity - 200 meters per second.

A lunar viewing loss of 0.5

where:

$$\text{Viewing loss} = \frac{1 - \cos \Theta}{2}$$

$$\sin \Theta = R / R + H$$



R = Radius of shielding body

H = Height above the lunar surface (Kilometers)

The Herrmann and Jones (Reference 41) penetration criteria slightly modified is used to predict the effect of lunar secondary activity. Generally, Herrmann and Jones examined a large body of already existing experimental data and found excellent correlation with the following expression.

$$\frac{P}{d} = B_1 \log_e \left( 1 + \frac{\rho_t V^2}{B_2 H_t} \right)$$

where:

p = crater depth in a quasi - infinite target

d = projectile diameter (centimeters)

$\left. \begin{matrix} B_1 \\ B_2 \end{matrix} \right\}$  = constants (determined experimentally)

$\rho_t$  = target density

$H_t$  = target Brinell hardness

$V$  = projectile impact velocity

The constants  $B_1$  and  $B_2$  are dependent upon the projectile and target materials and are determined empirically from data obtained from many projectile-target material combinations. Values  $B_1$  and  $B_2$  were derived for aluminum and steel impacted by borosilicate glass projectiles and are as follows:

Projectile	Target	$B_1$	$B_2$
Borosilicate Glass	Aluminum	0.854	37.5
	Steel	0.511	69.4

Borosilicate glass should closely approximate secondary particle density resulting from preliminary meteoroids impacting the lunar surface.

Quasi-infinite data obtained by posever and scully (Reference 42) when correlated to the penetration criteria proposed by Herrmann and Jones and Charters - Summers (Reference 40) was found to show remarkable agreement with Bjork's theory at high velocities and Maiden's theory at lower velocities approaching 9 kilometers per second. This is especially significant in that Maiden and Bjork's treatments were primarily theoretical.

Kinard et al (Reference 43) relates penetration produced in quasi-infinite targets to perforations of single sheets. The single-sheet thickness,  $t_s$ , was determined to be

$$t_s = 1.55 P$$

This value was further substantiated by Posever and Scully (Reference 42).

The mass,  $m$ , may now be substituted in the Herrmann and Jones equation for the particle diameter,  $d$ . Since the particle is assumed spherical,

$$v = \frac{1}{6} \rho_p d^3$$

$$\frac{m}{\rho_p} = \frac{1}{6} \rho_p d^3$$

or

$$d = \frac{6m}{\rho_p}^{1/3}$$

As previously noted, we describe the basic flux model for lunar secondary particles as:

$$\log_{10} F_s = -1.34 \log_{10} m - 6.59$$

where:

$F_s$  = the mean number or frequency of secondary impacts per square foot of the effected structure surface per day with mass equal to or greater than  $m$  grams

Transposing and solving for  $m$  in our flux equation we get the following:

$$\log F_s = -1.34 \log m - 6.59$$

$$\bar{N} = F_s A t$$

where:

$\bar{N}$  = the average number of impingements of particles with masses greater than or equal to  $m$  on a structure with surface area  $A$  feet square during a period  $t$  days long.

$$Fs = A \log (-1.34 \log m - 6.59)$$

$$\bar{N} = Fs At = At A \log (-1.34 \log m - 6.59)$$

$$\log \bar{N} = \log At - 1.34 \log m - 6.59$$

$$M = \left( \frac{At}{10^{6.59} \bar{N}} \right)^{\frac{1}{1.34}}$$

Substituting for particle diameter  $d$  in the Herrmann and Jones equation we get:

$$P = \beta_1 \left[ \log_e \left( 1 + \frac{\rho_t v^2}{\beta_2 H_t} \right) \right] \left( \frac{6m}{\rho \rho_p} \right)^{1/3}$$

Substituting for lunar secondary particle mass  $m$  in the above equation we get:

$$P = \beta_1 \left[ \log_e \left( 1 + \frac{\rho_t v^2}{\beta_2 H_t} \right) \right] \left( \frac{6}{\rho \rho_p} \right)^{1/3} \left( \frac{At}{10^{6.59} \bar{N}} \right)^{\frac{1}{4.02}}$$

Introducing the 1.5 penetration parameter, by substitution we obtain the expression for  $t_s$ , the single sheet thickness of the shield, as follows:

$$t_s = 1.5 P \left[ \log_e \left( 1 + \frac{\rho_t v^2}{\beta_2 H_t} \right) \right] \left( \frac{6}{\rho \rho_p} \right)^{1/3} \left( \frac{At}{10^{6.59} \bar{N}} \right)^{\frac{1}{4.02}}$$

For the probability of occurrence of a specified number of penetrations per unit of time, an accepted method of approach employs the mathematical Poisson model. In terms of the average number of impingements  $\bar{N}$ , the probability  $P(N)$  of  $N$  penetrations is:

$$P(N) = \frac{1}{\bar{N}!} \left[ \frac{N}{(\bar{N})} (e)^{-\bar{N}} \right]$$

Setting requirements for no penetrations we get:

$$P(0) = e^{-\bar{N}}$$

or

$$\log_e P(0) = -\bar{N}$$

By substituting in the equation for single sheet thickness we obtain a final relation by which the optimum single sheet design may be obtained for protection from lunar secondary particles, given the structure area, lunar stay time, and the probability of no penetration desired. The equation may be solved for any material for which density  $\rho_t$ , and Brinell hardness  $H_t$ , is known. As previously noted, the density of the lunar secondary particle  $\rho_p$  is assumed as 2.5 grams per cubic centimeter and particle velocity  $V$  is set at 200 meters per second or 0.2 kilometers per second. Values for  $\beta_1$ ,  $\beta_2$  for aluminum and steel are given in the first part of this section.

$$t_s = 1.5 \beta_1 \left[ \log_e \left( 1 + \frac{\rho_t V^2}{\beta_2 H_t} \right) \right] \left( \frac{6}{\pi \rho_p} \right)^{1/3} \left( \frac{At}{-10^{6.59 \log_e P(o)}} \right)^{\frac{1}{4.02}}$$

When solutions are obtained from the above equation the numerical values must be in units as listed below.

- (a) Target density ( $\rho_t$ ) - grams per cubic centimeters
- (b) Particle density ( $\rho_p$ ) - grams per cubic centimeters
- (c) Particle velocity ( $V$ ) - kilometers per second
- (d) Brinell Hardness ( $H_t$ ) - kilograms force per millimeter squared
- (e) Target thickness ( $t_s$ ) - centimeters
- (f) Exposed Structural Area ( $A$ ) - square feet
- (g) Lunar stay time ( $t$ ) - days

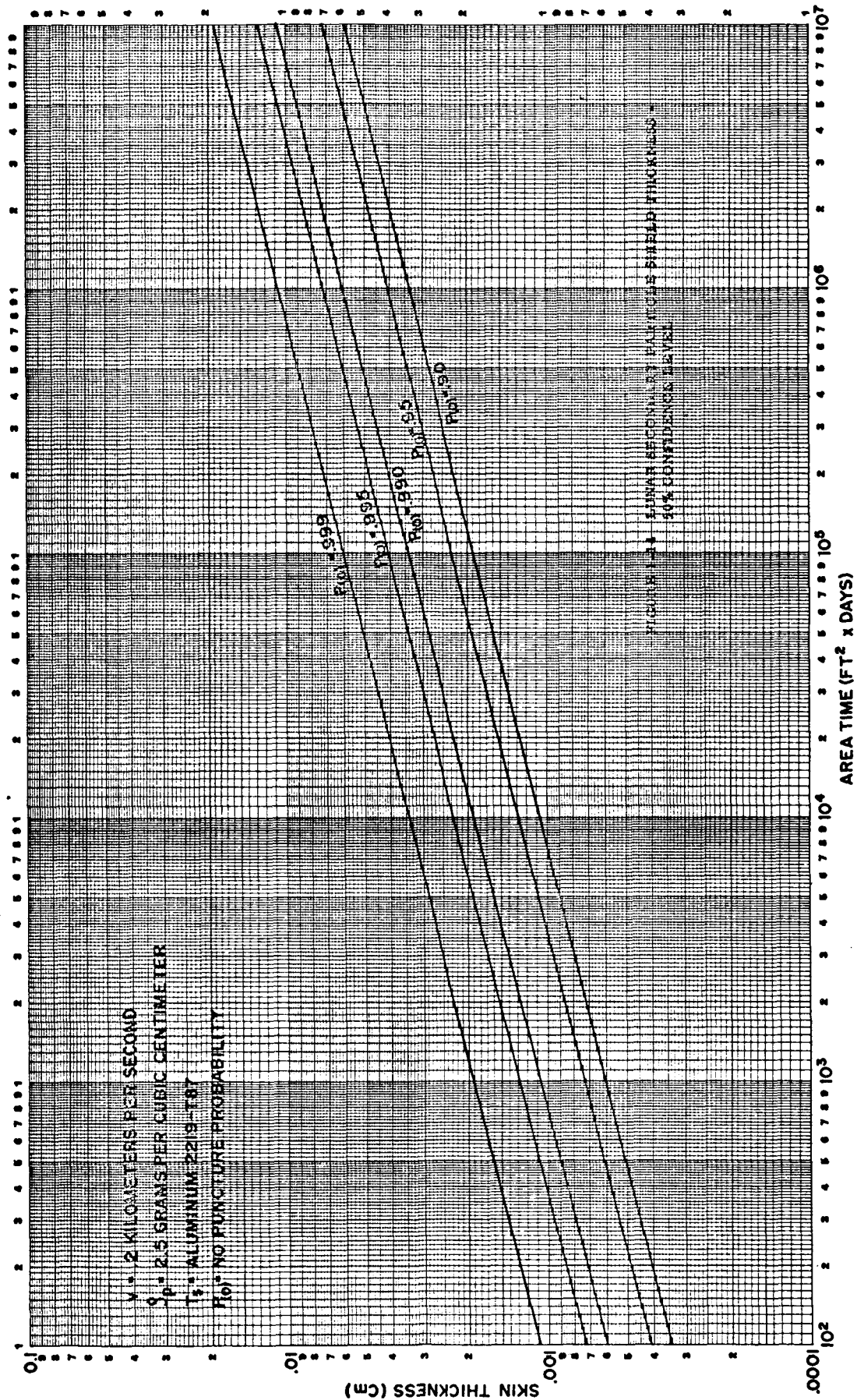
When using units as noted, a further proportionality constant ( $K$ ) is required to compensate for the difference in units used for Brinell hardness ( $H_t$ ), target density ( $\rho_t$ ), and particle velocity ( $V$ ). The proportionality constant  $K$  is defined as follows:

$$K = \frac{(\text{gm/cm}^3) (10^5 \text{ cm/sec})^2}{(980,665 \text{ gm cm/sec}^2) / (10^{-1} \text{ cm})^2} = 102$$

Our design equation now becomes:

$$t_s = 1.5 \beta_1 \left[ \log_e \left( 1 + K \frac{\rho_t V^2}{\beta_2 H_t} \right) \right] \left( \frac{6}{\pi \rho_p} \right)^{1/3} \left( \frac{At}{-10^{6.59 \log_e P(o)}} \right)^{\frac{1}{4.02}}$$

Figure 1-14 illustrates the single-sheet homogeneous wall thickness of Aluminum 2219-T87 required to protect a lunar structure from the lunar secondary environment. No puncture probabilities of .999, .995, .990, .95, and .90 were considered.





### 4.5.3 LUNAR AND NEAR LUNAR PRIMARY METEOROID FLUX AND PUNCTURE MODEL

The following treatment of the theoretical meteoroid flux and penetration criteria is based on basic models presented in reference 44.

#### (a) Cumulative impact flux on a total sphere

$$F_s = 10^{-14.54 \pm 0.60} m B_2$$

where

$F_s$  = the mean number of primary impacts per square meter of the exposed structure per second with mass equal to or greater than  $m$  grams.

$$B_2 = - \left[ 1.00 + (0.34) \left( \frac{h}{100} \right)^{0.113} - 0.24 \log \left( \frac{h}{100} \right) \right]$$

$h$  = height in kilometers above the earth

assuming

$\log \rho = \overline{\log \rho} \pm 0.30$  (i.e.,  $\overline{\log \rho} = (\log 0.44) \pm 0.30$ ) = meteoroid specific gravity

$\log V = \log 19.4 \pm 0.12$  = meteoroid velocity in kilometers per second.

To identify an equation which will give us the number of meteoroid impacts per square meter of structural surface on the lunar surface, the relation  $B_2$  is solved for the lunar distance i.e.,  $h = 3.84 \times 10^5$  kilometers.

$$\begin{aligned} B_2 &= - \left[ 1.00 + (0.34) \left( \frac{3.84 \times 10^5}{100} \right)^{0.113} - 0.24 \log \left( \frac{3.84 \times 10^5}{100} \right) \right] \\ &= - \left[ 1.00 + (0.34) (3,840)^{0.113} - 0.24 \log (3,840) \right] \\ &= - \left[ 1.00 + (0.34) (2.541) - 0.24 (3.58433) \right] \\ &= - (1.00 + .864 - .860) \end{aligned}$$

$$B_2 = - 1.004$$

For the lunar distance our basic flux equation becomes

$$F_s = 10^{-14.54 \pm 0.60} \bar{m}^{-1.004}$$

(b) Puncture Flux

$$\Phi = 10^{-13.84} \bar{m}^{B_2}$$

where

$\bar{m}$  = mass in grams of a nominally puncturing meteoroid

$$\bar{m} = 10^{11.193 \pm 0.45} (PC_t^{0.50} E_t^{1.31} V_t^{8.0} \epsilon_t^{0.43})^3$$

$\Phi$  = number of punctures of a randomly oriented vehicle per square meter of exposed area per second.

and

$p$  = thickness of a homogeneous metallic wall in centimeters

$C_t$  = Bulk velocity of sound in kilometers per second

$E_t = 10^{-6}$  times Young's modulus in kilograms per square centimeters

$\epsilon_t$  = ductility (percent elongation in 2-inch gauge length at fracture)

$V_t$  = Poisson's ratio

For the lunar distance our puncture flux equation becomes

$$\Phi = 10^{-13.84} \bar{m}^{-1.004}$$

where

$$\bar{m} = 10^{11.193 \pm 0.45} (PC_t^{0.50} E_t^{1.31} V_t^{8.0} \epsilon_t^{0.43})^3$$

The following derivation is made to arrive at a single equation which may be used to determine the skin thickness required to prevent puncture of a structure with a set statistical zero puncture probability, and with surface area  $A$  for a mission duration  $t$ .

$$\bar{N} = \Phi At$$

where

$\bar{N}$  = the average number of punctures of particles with mass equal to or greater than  $m$  grams, through the skin of a structure with surface  $A$  square meters during a mission duration  $t$  seconds long. Relations are established at the lunar distance.

$$\bar{N} = \Phi At = At 10^{-13.84} \frac{m}{m}^{-1.004}$$

For the probability of occurrence of a specified number of penetrations per unit of time, an accepted method of approach employs the mathematical poisson model. In terms of the average number of penetrations  $\bar{N}$  of a given structure the probability  $P(N)$  of  $N$  penetrations is:

$$P(N) = \frac{1}{N!} \left[ \frac{N!}{(\bar{N})^N} e^{-\bar{N}} \right]$$

Setting the requirement for Zero penetration we get:

$$P(0) = e^{-\bar{N}}$$

or

$$\log_e P(0) = -\bar{N}$$

Substituting in our penetration flux equation for the average number of penetrations for a given structure at the lunar distance we get:

$$-\log_e P(0) = At 10^{-13.84} \frac{m}{m}^{-1.004}$$

where:

$$m = 10^{11.193 \pm 0.45} (PC_t^{0.50} E_t^{1.31} V_t^{8.0} \epsilon_t^{0.43})^3$$

For Aluminum 2219-T87

$$C_t = 5.075 \text{ Kilometers/Sec}$$

$$E_t = .745 \text{ Kilograms/cm}^2$$

$$V_t = .325$$

$$\epsilon_t = 5\%$$

Consequently, for Aluminum 2219-T87 the meteoroid mass required to penetrate a thickness  $p$  centimeters is as follows:

$$m = 10^{11.193 \pm 0.45} (p^{5.075^{0.50} .745^{1.31} .325^{8.0} .05^{0.43}})^3$$

$$= 10^{11.193 \pm 0.45} (p^3 .0143 \times 10^{-11})$$

For a 75% confidence level  $\pm 0.45 \rightarrow -0.45$ . For a 50% confidence level  $\pm 0.45 \rightarrow 0$ . The latter will be treated first.

$$m = 10^{11.193} (.0143 \times 10^{-11} P^3)$$

$$m = .0223 P^3$$

Our penetration flux equation now becomes:

$$-\log_e P(o) = At 10^{-13.84} (.0223 P^3)^{-1.004}$$

$$-\log_e P(o) = At (10^{-13.84}) (.0223^{-1.004}) (P^{-3.012})$$

$$= At (.145 \times 10^{-13}) (45.54) (P^{-3.012})$$

$$= At (6.603 \times 10^{-13}) (P^{-3.012})$$

$$-\log_e P(o) = At (6.603 \times 10^{-13}) (P^{-3.012})$$

$$-\log_e P(o) = At \frac{(6.603 \times 10^{-13})}{P^{3.012}}$$

$$P^{3.012} = \left[ \frac{At}{\log_e P(o)} \right] 6.603 \times 10^{-13}$$

$$P = -9.039 \times 10^{-5} \left[ \frac{At}{+ \log_e P(o)} \right] .3320$$

Where p represents the single sheet homogeneous wall thickness in centimeters of AL 2219-T87 required to prevent penetration of a Lunar Structure A square meters in area, for a mission duration of t seconds, at a no puncture probability level of P(o). The confidence level is established at 50 percent i.e., numerically speaking there is an even chance that the true values will fall to either side of that from the prescribed equation. Figure 1-15 presents design curves for zero puncture probabilities of .90, .95, .990, .995 and .999.

The following constitutes treatment of our original equation to provide a 75% confidence level.

$$m = 10^{11.193 - 0.45 (P^3 .0143 \times 10^{-11})}$$

$$m = .00791$$

Our penetration flux equation now becomes

$$-\log P(o) = At 10^{-13.84} (.00791 P^3)^{-1.004}$$

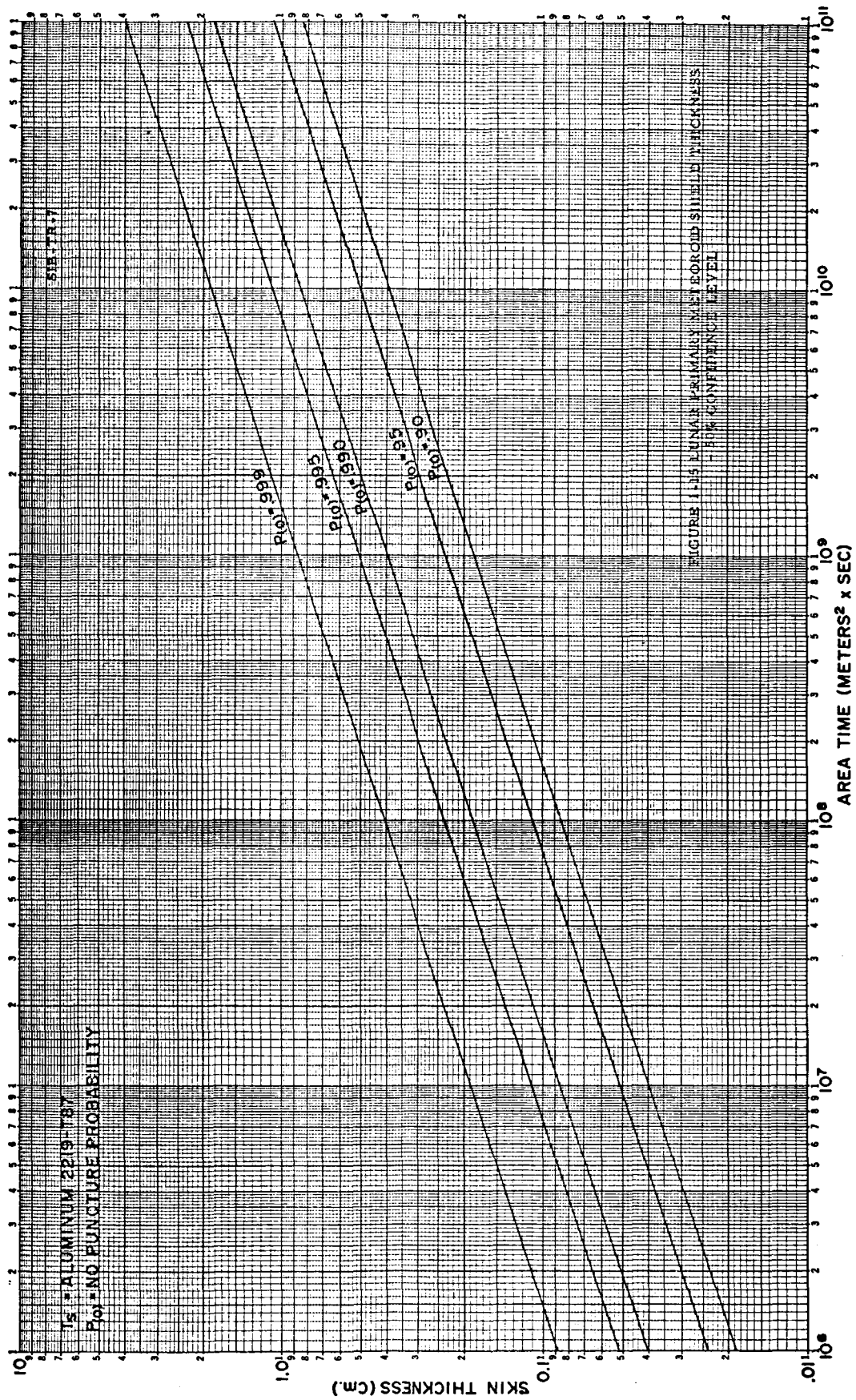
$$= At (.145 \times 10^{-13}) (.00791)^{-1.004} (P^{-3.012})$$

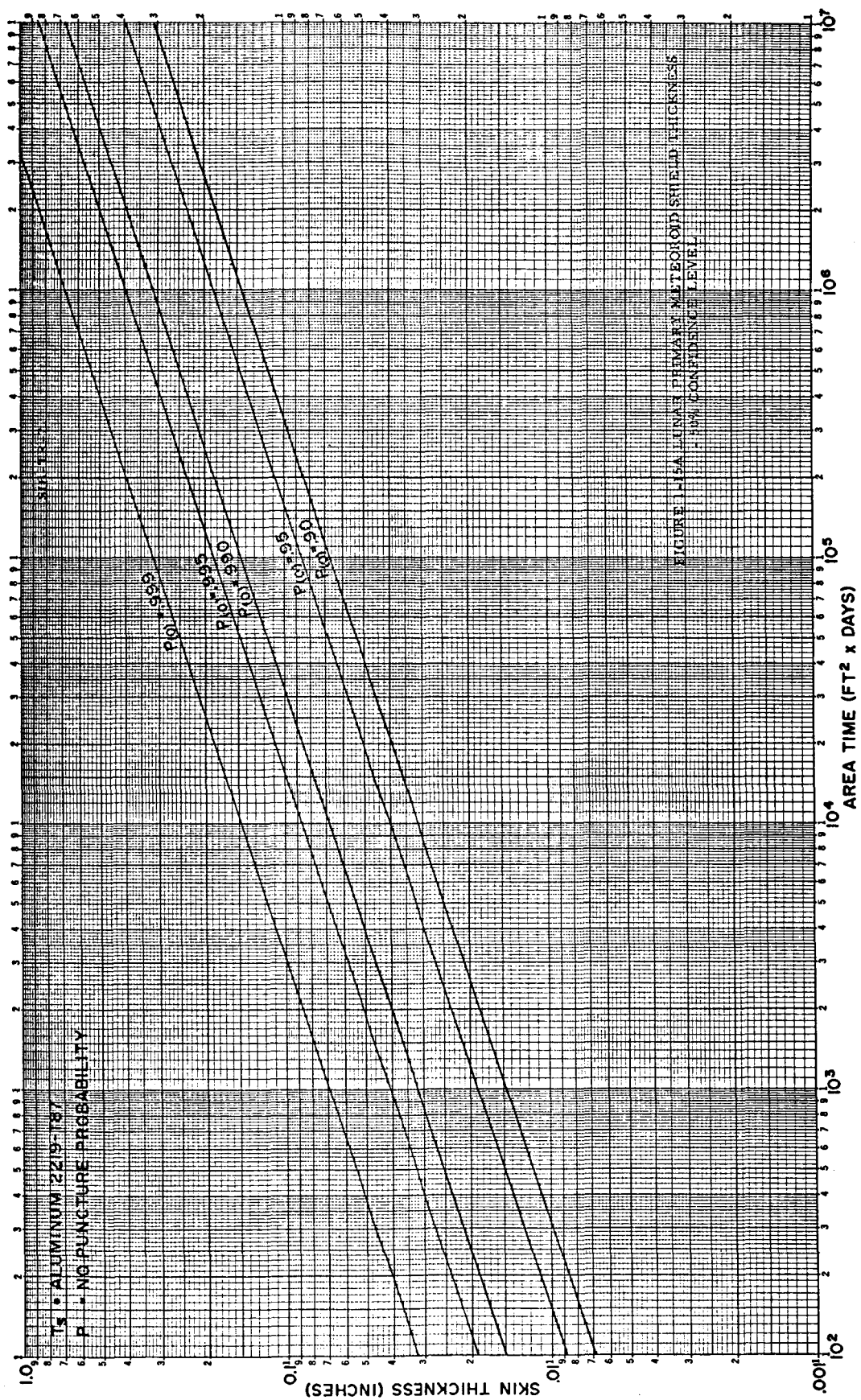
$$= At (.145 \times 10^{-13}) (128.8) (P^{-3.012})$$

$$-\log P(o) = At (1.868 \times 10^{-12}) P^{-3.012}$$

$$P^{3.012} = \left[ \frac{At}{-\log_e P(o)} \right] 1.868 \times 10^{-12}$$

$$P^{-1.278 \times 10^{-4}} \left[ \frac{At}{+ \log_e P(o)} \right] .3320$$





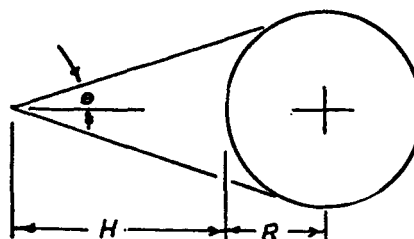
Where  $p$  represents the single sheet homogeneous wall thickness in centimeters of AL 2219-T87 required to prevent penetration of a Lunar Structure  $A$  square meters in area for a mission duration  $t$  seconds, at a no puncture probability of  $P(0)$ , the confidence level is established at 75 percent. Figure 1-16 presents design curves for zero puncture probabilities of .90, .95, .990, .995, and .999. However, before using the design curves, an appropriate viewing loss imposed by the moon must be considered.

On the lunar surface a viewing loss of 0.5 would be used, i.e., the total exposed structural area of the Lunar structure would be reduced by a factor of 2 before the required skin thickness is obtained from the design curves. For other positions above the lunar surface the following procedure would be used.

$$\text{Viewing loss} = \frac{1 - \cos \Theta}{2}$$

where

$$\sin \Theta = \frac{R}{R + H}$$



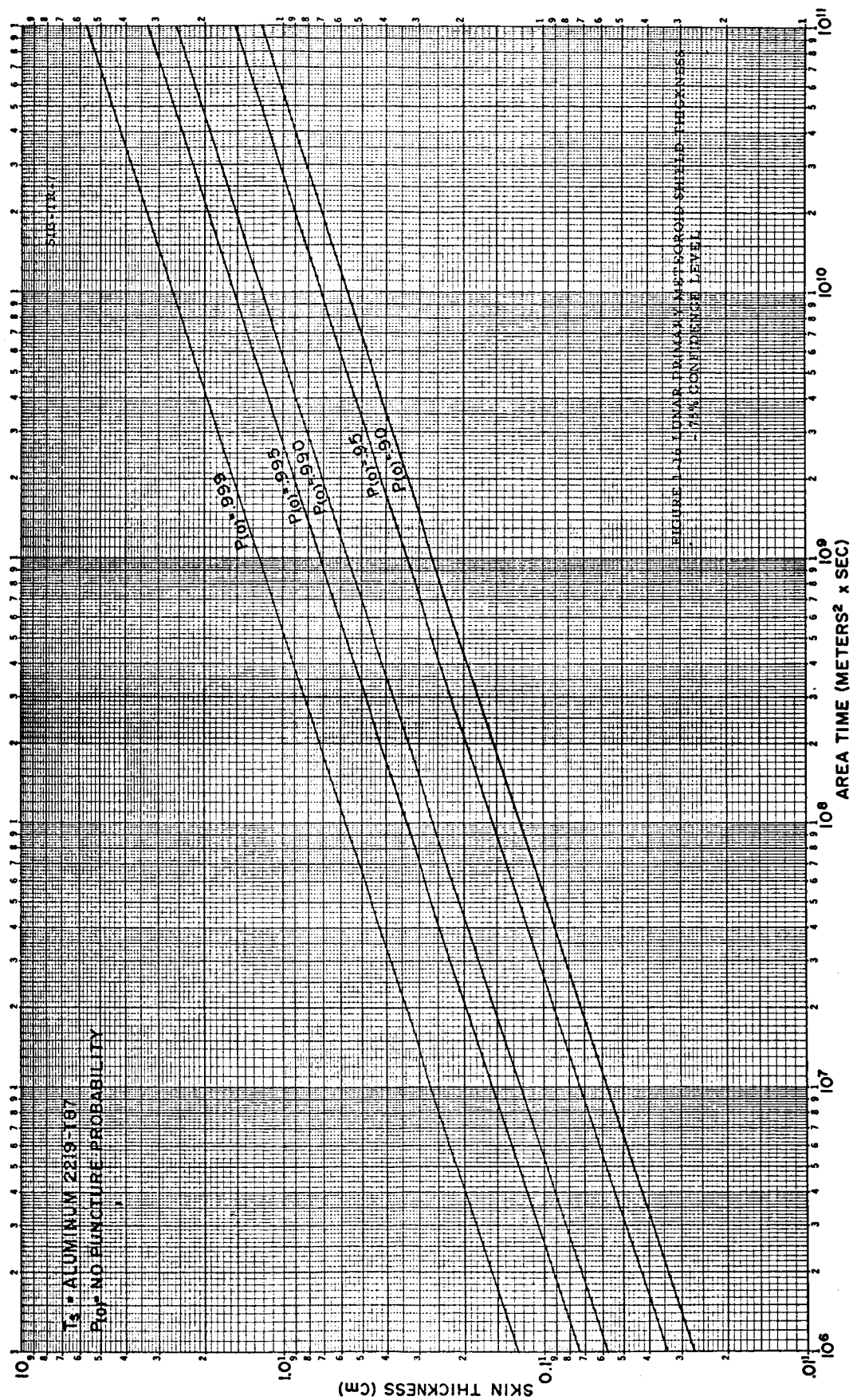
#### 4.6 SINGLE-MULTIPLE SHEET METEOROID SHIELDING CORRELATION

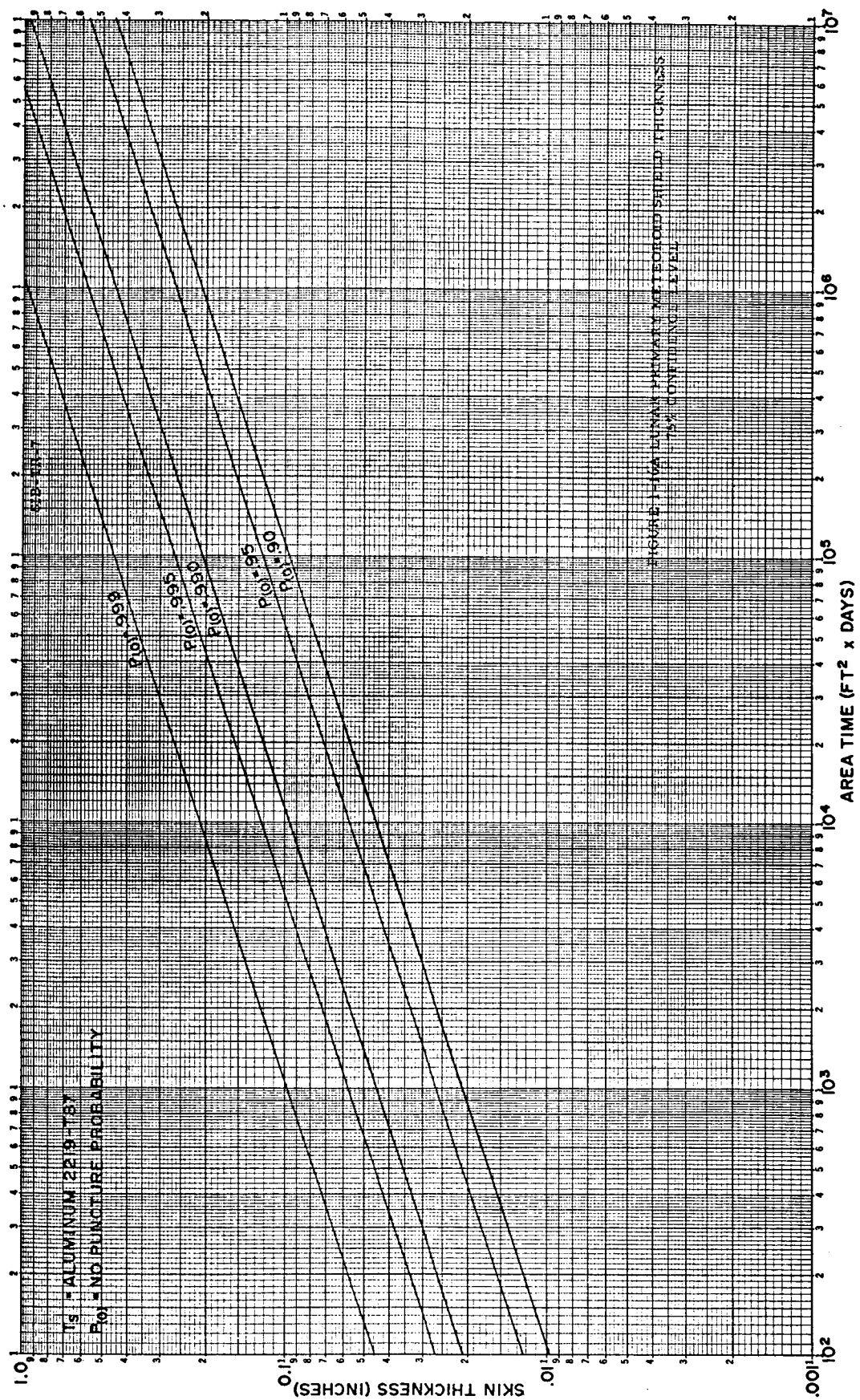
The preceeding three sections have outlined the procedures to obtain the thickness of a single sheet of Aluminum 2219-T87 required to protect a structure from the near-earth, cislunar, and lunar meteoroid environment. Previously it has been shown, with supporting references, that the optimum meteoroid shielding design is a multiple sheet structure. Consequently, the problem remains of transferring from a single-sheet to an equivalent effective multiple-sheet structure.

The Ames Research Center per reference (15) provides the key to the transfer from a single to a multiple sheet structure. The assumption is made that the ratio  $R$  of the ballistic limits, holds constant for all conditions of impact.

$$\frac{V_m}{V_s} = R = \text{constant}$$







Where  $V_m$  is the ballistic limit of the multiple-sheet target and  $V_s$  is the ballistic limit of the single sheet target. The ballistic limit is defined as the velocity at which complete target penetration is just prevented.

Figure 1-17 represents ballistic limit data obtained experimentally by Reference (15). The method employed single and multiple-sheet structures constructed of 2024-T3 Aluminum Alclad. The number of sheets and thicknesses were varied so that all times the total thickness always had one value of 0.062 inches. Thus, the weight per unit area was held constant. The number of sheets in Figure 1-17 varied from one to four. In this particular example, two values for sheet spacing was used. ( $1/2''$  and  $1''$ ) with the spacing between successive sheets being held constant.

Figure 1-17 also shows the effect of glass wool filler application to the  $1''$  spaced two sheet target.

For purposes of discussion we shall now compare the ballistic limit of a single sheet target versus that of two sheets spaced 1 inch apart and filled with glass wool. From Figure 1-17 we find  $R$  to be,

$$R = \frac{V_m}{V_s} = \frac{11,050 \text{ ft/sec.}}{2,400 \text{ ft/sec.}} = 4.4 \text{ or } .228$$

In effect, this relation says that the two sheet glass wool filled target is 4.4 times better than the single sheet target assuming the metal weight per unit area is the same for both cases.

If one calculated the single sheet thickness required to protect a structure from the near-earth, cislunar, and lunar meteoroid environment and divided it by the ratio  $R$ , of the ballistic limits, the resultant figure would constitute the equivalent effective thickness of the multiple-sheet structure being compared.

Now that we have identified the mechanics of transfer from a single-sheet to a multiple-sheet we define a unit called the Effectiveness Factor ( $K$ ) which is derived from the ratio  $R$ .

$$K = \frac{1}{R} = \frac{V_s}{V_m}$$

Figure 1-18 shows the effectiveness factors for several multiple-sheet meteoroid shield configurations. The type desired may be selected and the effectiveness factor  $K$  applied to the following relation to obtain the bumper sheet thickness.

$$t_{\text{eff}} = \frac{N \bar{t}}{K}$$

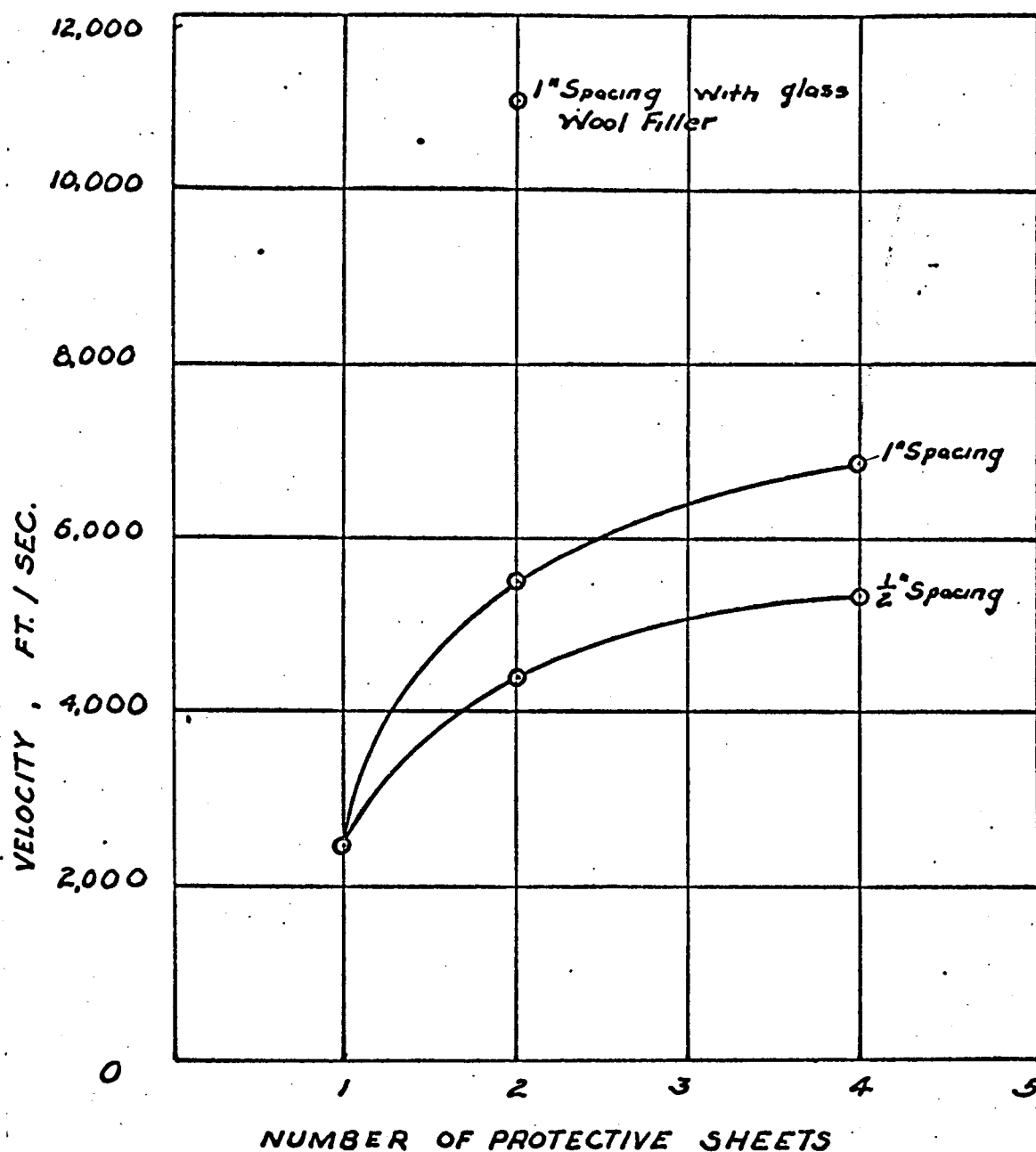


FIGURE 1-17 VARIATION OF TARGET BALLISTIC LIMIT AS A FUNCTION OF THE NUMBER OF PROTECTIVE SHEETS

Where:

$N$  = the number of sheets blocking the path of a particle penetrating a multiple-sheet structure

$\bar{t}$  = thickness of individual structural sheets which together comprise a multiple-sheet meteoroid shield

$K$  = Effectiveness factor

$t_{\text{eff}}$  = the effective single sheet armorplate shield thickness

For a given structure,  $\bar{t}$  denotes the thickness of the bumper and any other sheet designed to block the path of an impacting projectile including the main pressure vessel wall. However, per reference (32) the limiting design factor for the main pressure vessel wall for manned structures is the internal working pressure. Per reference (32) the thickness required to contain a human operating environment far exceeds that required for meteoroid shielding purposes. Consequently, the calculated value for  $\bar{t}$  would represent a minimum value for the main pressure vessel wall.

#### 4.7 CONCLUSIONS - MICROMETEOROID SHIELDING DESIGN

It is significant to note that the procedure used to arrive at a meteoroid shielding design is flexible. It may be used to determine the effectiveness of any number of protective sheets in combination with fillers, providing the ballistic limit is known.

Spallation is a factor inherent in the value of the ballistic limit and need not be considered further. Were spallation a factor which caused failure of the target, it would have served to lower the value of the ballistic Limit. The definition of the ballistic limit being that velocity at which penetration of a target is just prevented.

Future efforts applied toward the study of meteoroid shielding design which would be of benefit are listed.

- (1) Analysis of the results of experimental studies performed with new high velocity guns to determine if the ratio

$$R = \frac{V_m}{V_s} \text{ remains constant.}$$

- (2) Review of experimental data to determine the ballistic limits of two sheet meteoroid shielding spaced beyond 1 inch using varying types of filler material.

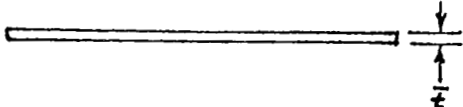
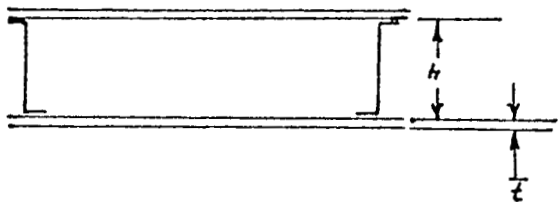
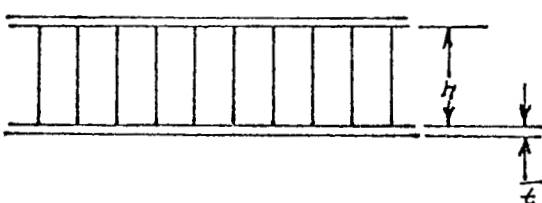
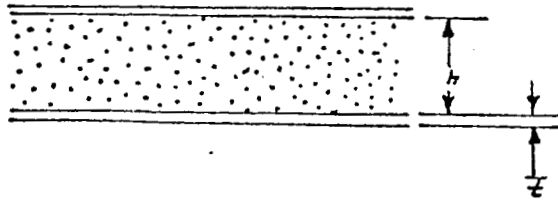
	h	k
	—	1.0
 <p>TWO SHEET - NO FILLER</p>	1.0" space 1.5" space 2.0" space	0.50 0.35 0.20
 <p>HONEYCOMB CORE- NO FILLER</p>	1.0" space 1.5" space 2.0" space	0.50 0.40 0.33
 <p>GLASS WOOL FILLER</p>	1.0" space	0.23

FIGURE 1-18 METEOROID SHIELDING EFFICIENCY FACTORS

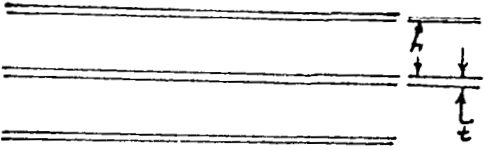
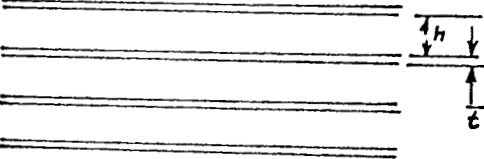
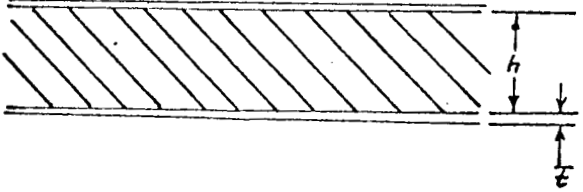
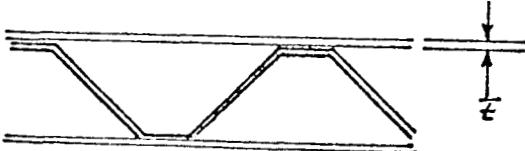
	h	k
 <p>THREE SHEET WITH NO FILLER</p>	1/2" space 1" space	0.48 0.38
 <p>FOUR SHEET WITH NO FILLER</p>	1/2" space 1" space	0.45 0.35
 <p>LOW DENSITY POROUS PLASTIC CORE</p>	1.0" space 1.5" space 2.0" space	0.33 0.25 0.14
 <p>NO FILLER</p>	—	0.20

FIGURE 1-18 (CONT) METEOROID SHIELDING EFFICIENCY FACTORS

# SECTION 5.0 REFERENCES

1. Whipple, Fred L.                      The Meteoritic Risk to Space Vehicles  
Paper 499-57, Am Rocket Soc., Inc.,  
1957.
2. Summers, James L.                  Investigation of High-Speed Impact:  
Regions of Impact and Impact at  
Oblique Angles NASA TN D-94, 1959
3. Whipple, Fred L.                      Meteoritic Phenomena and Meteorites.  
Physics and Medicine of the Upper At-  
mosphere, Clayton S. White and Otis  
O. Benson, Jr., eds., The Univ. of  
New Mexico Press (Albuquerque),  
1952 137-170.
4. Humes, Donald H.                    An Experimental Investigation of the  
Effectiveness of Single Aluminum  
Meteoroid Bumpers, NASA TN D-1784,  
1964.
5. Kinard, William H.  
Lambert, C. H., Jr.  
Schryer, David R.  
Casey, Francis W., Jr.                Effect of Target Thickness on Cratering  
and Penetration of Projectiles Impacting  
at Velocities to 1,300 Feet per Second.  
NASA Memo 10-18-58L, 1964.
6. Collins, Rufus D., Jr.  
Kinard, William H.                    The Dependency of Penetration of the  
Momentum per Unit Area of the Im-  
pacting Projectile and the Resistance  
of Materials to Penetration. NASA  
TN D-238, 1960.
7. Davidson, Elmer  
Winslow, Paul C., Jr.                Direct Evaluation of Meteoroid Hazard  
Aerospace Eng., Volume 21, Feb 1962,  
pp. 24-33.
8. Gallagher, P. B.                    "Sporadic Shower" properties of Very  
Small Meteors Jour. Geophys. Res.,  
Vol. 65, No. 6, June 1960, pp. 1846-1847.
9. Staff of the Lewis  
Research Center                      Micrometeoroid Satellite (Explorer XIII)  
Stainless Steel Penetration Rate Experi-  
ment, NASA TN D-1986 October 1963.
10. Davison, Elmer H.  
Winslow, Paul C., Jr.  
Lewis Research Center                Micrometeoroid Satellite (Explorer XVI)  
Stainless Steel Penetration Rate Experi-  
ment. NASA TN D-2445, August 1964.



11. Summers, James L. Investigation of High-Speed Impact - Regions of Impact and Impact at Oblique Angles. NASA TN D-94, 1959.
12. Nysmith, C. Robert  
Summers, James L. An Experimental Investigation of the Impact Resistance of Double-Sheet Structures at Velocities to 24,000 Feet per Second - NASA TN D-1431.
13. Whipple, F. L. "On Meteoroids and Penetration", Journal of the Astronautical Sciences, Vol. X, No. 3, pp 92-94, Fall 1963.
14. Dalton, C. C. "Estimation of Tolerance Limits for Meteoroid Hazard to Space Vehicles" NASA TN D-1996, February 1964.
15. Nysmith, C. Robert  
Summers, James L. "Preliminary Investigation of Impact on Multiple-Sheet Structures and An Evaluation of the Meteoroid Hazard to Space Vehicles" NASA TN D-1039
16. P. E. Sandorff "A Meteoroid Bumper Design Criterion" Proceedings of the 6th Symposium on Hyper-velocity Impact - Cleveland April 30 - May 2, 1963, Vol. 3, August 1963.
17. Vaughan, William W. Lunar Surface Primary Meteoroid Flux and Puncture Model for Lunar Mobile Laboratory (LMOL) Studies. R-AERO-Y-26-64. April 22, 1964 - George C. Marshall Space Flight Center
18. Carlson, R. E.  
Fager, J. A. Effects of Hypervelocity Impact on Semi-infinite Plate and Composite Spacecraft Hulls from 18,000 FPS to 100,000 FPS - Preprint of a paper presented to AIAA 6th Structures & Material Conference April 5, 1965.
19. Maiden  
McMillan An Investigation of the Protection Afforded a Spacecraft by a Thin Shield. A presentation made at the AIAA Aerospace Sciences Meeting. New York, N. Y., 1964.

20. Posover  
Scully Investigation of Structural Implications of Meteoroid Impact. Air Force Flight Dynamics Laboratory, Research and Technology Division, Wright-Patterson Air Force Base. Report No. FDL TDE-64-96 dated July 1964.
21. Walsh  
et al Summary Report on the Theory of Hypervelocity Impact - General Dynamics/General Atomic Report No. GA5119, 31 March 1964.
22. Rhodes  
Bloxsom MOL Hypervelocity Impact Testing - Report II-6, Document 210-SC-5A, 26 July 1964.
23. Rhodes  
Bloxsom Penetration Testing of Scale Hull, GD/A MOL System at 28,500 to 90,000 FPS Velocities, 15 September 1964.
24. Rhodes  
Bloxsom Penetration Testing of Scale Hull, GD/A MOL System - Report No. MP-64-1, 7 October, 1964.
25. MIL-HDBK-5 Revised 1 May 1964
26. Brooks &  
Perkins, Inc. Specification BP-S-125, Revision B, Magnesium-Lithium Alloy Sheet and Plate (LA 141A).
27. Smith Analytical Techniques for the Determination of Meteoroid Protection Requirements - General Dynamics/Astronautics Report No. GD/A 63-1408, 31 Dec 1963.
28. Frost Aerospace Meteoroid Environment and Penetration Criterion - Aerospace Corporation Report No. TOR-269 (4560-40)-2, 17 August 1964.
29. Lundeberg, J. F.  
Stern, P. H.  
Bristow, R. J. Meteoroid Protection for Spacecraft Structures, Contract Number - NAS 3-2570, Dec 4, 1964.
30. Dalton, Charles C. Cislunar Meteoroid Impact and Puncture Models with Predicted Pegasus Satellite Punctures. NASA TM X-53187 dated January 13, 1965.

31. Whipple, F. L. On Meteoroids and Penetration - Journal of the Astronautical Sciences, Vol. X, No. 3, pp. 92-94, Fall 1963.
32. San Juan, E. C.  
Johnson, B. R., Jr.  
Curtiss, C. M. Lunar Shelter Design - Report by Brown Engineering Co. Inc. for the Base Development Group - Advanced Studies Office of Marshall Space Flight Center
33. Marshall Space Flight Center - Aero-Astrophysics Office Lunar Surface Primary Meteoroid Flux and Puncture Model for Lunar Mobile Laboratory (LMOL) Studies R-AERO-Y-26-64 dated April 22, 1964.
34. Marshall Space Flight Center - Aero-Astrophysics Office Near-Earth and Cislunar Meteoroid Flux and Puncture Model for use in MSFC Projects. R-AERO-Y-33-64 dated July 13, 1964.
35. Hawkins, G. S. Impacts on the Earth and Moon - Nature Magazine, Vol. 197, No. 4869, pp. 781, February 23, 1963.
36. Marshall Space Flight Center - Aero-Astrodynamic Laboratory Aero-Astrodynamic Research and Development Research Review No. 1 NASA TM X-53189 dated October 1, 1964.
37. Manned Spacecraft Center - Manned Spacecraft Criteria and Standards Board Meteoroid Environment in Near-Earth, Cislunar, and Near-Lunar Space - EC-1 dated November 8, 1963.
38. Gault, D. E.  
Shoemaker, E. M.  
Moore, J. H. Spray Ejected From the Lunar Surface by Meteoroid Impact - NASA Technical Note TN D-1767, April 1963.
39. Rodriguez, D. Meteoroid Shielding for Space Vehicles Aerospace Engineering, 1960.
40. Charters, A. C. A Preliminary Investigation of High-Speed Impact: The Penetration of Small Spheres into Thick Copper Targets - NASA RM A58B26 (1958).

41. Herman, W.  
Jones, A. H.      Survey of Hypervelocity Impact  
Information ASRL Report No. 99-1,  
Massachusetts Institute of Technology  
(1961).
42. Posover, F. C.  
Rish, F. L.  
Scully, C. N.      An Evaluation of Impact Effect on  
Meteoroid Shielding Configurations for  
Velocities up to 60,000 Feet per Second -  
AIAA Fifth Annual Structures and  
Materials Conference - April 1-3, 1964.
43. Kinard, W. H.  
Lambert, C. H., Jr.  
Schryer, D. R.  
Casey, F. W., Jr.      Effect of Target Thickness on Cratering  
and Penetration of Projectiles Impacting  
at Velocities to 13,000 Feet per Second -  
NASA Memo 10-18-58L (1958).
44. Smith, R. E.      Space Environment Criteria Guidelines For  
Use In Space Vehicle Development NASA  
TM X-53273, May 27, 1965.
45. Maiden, C. J.  
McMillan, A. R.,  
Sennett, R. E.,  
Gehring, J. W.      TR 65-48 Experimental Investigations of  
Simulated Meteoroid Damage to Various  
Spacecraft Structures - GM Defense Re-  
search Laboratories - July 1965.